1 Organic geochemical investigations of an MIS 5 fire in the

2 Palaeolithic deposits of Ormesson (Seine-et-Marne, France):

3 Anthropic or natural?

- 4 Ivy Notterpek^{1,2,*}, Alexandre Lucquin¹, Samuel Abiven^{3,4}, Pierre Bodu⁵, Tobias Bromm⁶, Bruno Glaser⁶,
- 5 Henri-Georges Naton⁷, Matthew D. Pickering⁸, Oliver E. Craig¹, Isabelle Théry-Parisot²
- 6 ¹ BioArch, Department of Archaeology, University of York, Environment Building, Wentworth Way,
- 7 YO10 5NG, York, UK
- 8 ² Université Côte d'Azur, CNRS, CEPAM UMR 7264, SJA3, 24 Avenue des Diables Blue, 06300, Nice,
- 9 France
- 10 ³ Laboratoire de Géologie, Département de Géosciences, CNRS Ecole Normale Supérieure, PSL
- 11 Université, Institut Pierre Simon Laplace, 24 rue Lhomond, 75005, Paris, France
- ⁴ CEREEP-Ecotron lle De France, CNRS Ecole Normale Supérieure, PSL Université, 11 Chemin de
- 13 Busseau, 77140, St-Pierre-lès-Nemours, France
- ⁵ UMR 8068 TEMPS, MSH Mondes Bâtiment Ginouvès, 21 Allée de l'Université, 92023, Nanterre
- 15 Cedex, France
- 16 ⁶ Institute of Agricultural and Nutritional Sciences, Soil Biogeochemistry, Martin Luther University
- 17 Halle-Wittenberg, Von-Seckendorff-Platz 3, 06120, Halle (Saale), Germany
- ⁷ GeoArchPal-GéoArchÉon, TEMPS UMR 8068, 30 Rue de la Victoire, 55210, Viéville-sous-les-Côtes,
- 19 France
- 20 8 Department of Environment and Geography, University of York, Environment Building, Wentworth
- 21 Way, YO10 5NG, York, UK
- 22
- * Corresponding author.
- 24 Email: ivynotterpek@palaeome.org
- 25
- Keywords: geochemistry; lipid biomarkers; benzene polycarboxylic acids; wildfire; Pleistocene; MIS 5;
- 27 combustion temperature

Abstract

29

30

31

32

33

34

35

36

37

38

39

40

41

42

43

44

45

46

47

48

49

50

51

52

Despite the central role of fire in Pleistocene and Palaeolithic lifeways, the relationship among hominins, fire, and their environment remains unclear. Ancient combustion residues hold a wealth of molecular data that may help to resolve some of these questions, yet standardised guidelines for reconstructing past fire traces are notably lacking. In this study, we examine extensive combustion residues overlying Middle Palaeolithic deposits from the open-air site of Ormesson (France). To determine whether the combustion residues are of natural or human origin, multiproxy approaches including anthracology, lipid biomarker, and benzene polycarboxylic acid (BPCA) analyses are applied. These techniques are used to characterise organic matter and pyrogenic carbon compositions in the deposits, providing insights into surrounding vegetation, palaeoenvironmental shifts, and the production parameters involved in the formation of the char assemblage. Lipid biomarker evidence suggests that the pre-fire local environment featured abundant coniferous vegetation (e.g., Pinaceae taxa), which is supported by anthracological evidence for a predominance of Pinus cf. sylvestris/nigra complemented by Betula sp. taxa. The post-fire environment saw a contraction of coniferous vegetation, concurrent with an expansion of deciduous taxa, grasses and herbaceous material. The combustion event, which resulted in 67% of the charcoal assemblage exhibiting vitrification, produced PyC contents of up to 362 g/kg OC in soil samples and 443 g/kg OC in charcoal samples, with aromatic condensation values of up to 34%. BPCA-derived predictions of heat treatment temperatures yielded values of approximately 300–400 °C for charcoal samples and 400–550 °C for soil samples in the burned layer, constituting the first instance in which quantitative temperature estimations are obtained from BPCA results. Based on the integrated evidence, we accept the null hypothesis that the studied combustion residues are natural in origin. However, the similarity of archaeometric and geochemical signatures from natural and human-controlled fires underscores the need for interdisciplinary, multiproxy efforts to improve the identification of past fire regimes.

1. Introduction

54

55

56

57

58

59

60

61

62

63

64

65

66

67

68

69

70

71

72

73

74

75

76

77

78

79

The habitual and controlled use of fire was integral to the evolutionary development of *Homo*, with numerous biological, social, and technological ramifications. However, the nature and chronology of hominin "habituation to natural fire, use of fire, maintenance of fire, [and] manufacture of fire" (Sandgathe, 2017: S367) remain clouded by regional variability and the often-fragmentary archaeological record of early sites (see also Gowlett, 2016). Evidence for fire use outside of Africa is limited prior to 0.5 Ma, and becomes markedly more frequent after 400 ka (Goren-Inbar et al., 2004; Fernández Peris et al., 2012; Shimelmitz et al., 2014; Rhodes et al., 2016; Rosell and Blasco, 2019; Sanz et al., 2020; Stancampiano et al., 2023). This intensification may signal the emergence of fire production techniques, rather than the control or maintenance of natural fires, as suggested for earlier contexts (Roebroeks and Villa, 2011; Sandgathe, 2017). Yet in the Middle Palaeolithic, evidence from Neandertal occupation sites in southwest France indicates that fire frequency was higher during warmer than colder periods; this pattern has been interpreted as opportunistic harvesting of naturally occurring fires, likely more common in warmer conditions (e.g., from lightning strikes), rather than independent fire generation (Sandgathe et al., 2011; Dibble et al., 2017, 2018). The ways in which Neandertals used fire (e.g., opportunistic vs. intentional), the technical skills involved (e.g., regulation vs. production), and the implications of these practices for behavioural complexity are subjects of ongoing debate, with direct relevance for understanding the development and diversification of pyrotechnology throughout the Pleistocene.

Resolving these debates requires rigorous analyses of archaeological fire traces at both macroand micro-scopic scales. Despite decades of multidisciplinary efforts, clear diagnostic guidelines have
yet to be established for one of the most essential aspects of reconstructing past fire: determining
natural or anthropogenic origins. The distinction of these fire types has been pursued through a
number of techniques, including: (i) palaeomagnetism and magnetic susceptibility (Barbetti, 1986;
Deldicque et al., 2021); (ii) charcoal reflectance values (McParland et al., 2009; Belcher et al., 2018;
Braadbaart et al., 2020); and (iii) the analysis of micro-material including microfaunal remains

(Fernandez-Jalvo and Avery, 2015; Rhodes et al., 2016) and flint debitage (Alperson-Afil, 2012). Researchers have also sought to discriminate these fire types via distributions of polycyclic aromatic hydrocarbons (PAHs) (Brittingham et al., 2019; Bird et al., 2024), or other molecular evidence (Wolf et al., 2013; Jambrina-Enríquez et al., 2019; Stancampiano et al., 2023). Lastly, these fire types have been investigated using temperature estimations (e.g., Marynowski et al., 2011; Walker et al., 2016), often derived through the comparison of ancient material (e.g., charcoal, bone) to thermally altered experimental references (Ferrio et al., 2006; Scott, 2010; Deldicque et al., 2016, 2023). These efforts are predicated on the notion that natural and anthropogenic fires burn at different combustion temperatures, with higher temperatures typically ascribed to human-controlled fires (e.g., Wolf et al., 2013). However in the majority of early-middle Pleistocene and lower-middle Palaeolithic sites, the association of fire traces with hominin activity is more often inferred from stratigraphic and chronological investigations (e.g., Berna et al., 2012; Stahlschmidt et al., 2015) rather than molecular techniques.

The full potential of molecular data in ancient fire traces thus remains largely underexploited, despite significant advances in the study of thermally altered organic matter (OM). Analyses of lipid biomarkers via organic residue analysis and of pyrogenic carbon (PyC) via benzene polycarboxylic acid (BPCA) analysis are particularly promising, as these methods target amorphous organic residues and molecular PyC that can persist far longer than macroscopic charred remains (e.g., Brocks et al., 2005; Kappenberg et al., 2019). Lipid biomarker analysis enables the reconstruction of biogenic sources and processes (Evershed, 2008), with applications ranging from identifying vegetal inputs to soil organic matter (SOM) (e.g., Schäfer et al., 2016) to detecting the organic signature of combustion features used for cooking meat (e.g., Lejay et al., 2019). BPCA analysis, which is one of several methods for characterising condensed aromatic moieties in PyC (Hammes et al., 2007), can be used to reconstruct char production parameters such as heat treatment temperature (HTT) (Glaser et al., 1998; Notterpek et al., 2025). The combined application of these methods to ancient combustion residues, particularly of uncertain origin, has not been reported. This study applies lipid biomarker and BPCA analyses to

combustion residues associated with Palaeolithic archaeological remains in order to assess the analytic and interpretive capabilities of these methods for characterising past fire traces.

Extensive burned deposits directly overlying a Middle Palaeolithic archaeological layer at the multi-stratified open-air site of Ormesson (Seine-et-Marne, north-central France) were analysed, as the anthropic or natural origins of the combustion traces were unknown. These combustion deposits could have resulted from human actions — whether through the deliberate burning of the site, the use of a large fire as a smoke signal, or the accidental spread of an unmanaged combustion feature. Alternatively, these deposits could testify to a previously unknown wildfire in the Paris basin region, or contain anthropogenic fire traces that were masked by a subsequent wildfire. As the natural or anthropic origin of the fire cannot be determined a priori, this study evaluated the following principal research question: Did these combustion residues result from a wildfire, or human activity? This question was addressed through the examination of: (i) anthracological evidence from the charcoal assemblage, including wood taxonomy and anatomical features indicative of the state of wood at the time of combustion; (ii) SOM composition and its implications for surrounding vegetation and palaeoclimatic conditions at the time of the event; (iii) PyC composition to reconstruct the combustion conditions in which the charred material was produced, namely HTT; and (iv) taphonomic and diagenetic alterations to the biomarker evidence. By detailing these factors through the integration of geological, anthracological, and geochemical data, this study highlights important considerations regarding the capabilities and constraints of geochemical and archaeological approaches for the interpretation of past fire traces.

2. Description of the study site

106

107

108

109

110

111

112

113

114

115

116

117

118

119

120

121

122

123

124

125

126

127

128

129

130

131

The site of Ormesson is located approximately 70 km southwest of Paris in a valley perpendicular to the Loing River (Lambert coordinates X: 624.1, Y: 1061.25) (Fig. S1). The site contains at least six Palaeolithic occupations, of which four are located on the eastern portion of the site (Les Bossats à Ormesson). These include Mousterian discoid (c. 42–46 ka cal BP), Châtelperronian (c. 42 ka cal BP), Gravettian (c. 31 ka cal BP), and Middle Solutrean (c. 23.5 ka cal BP) archaeological deposits

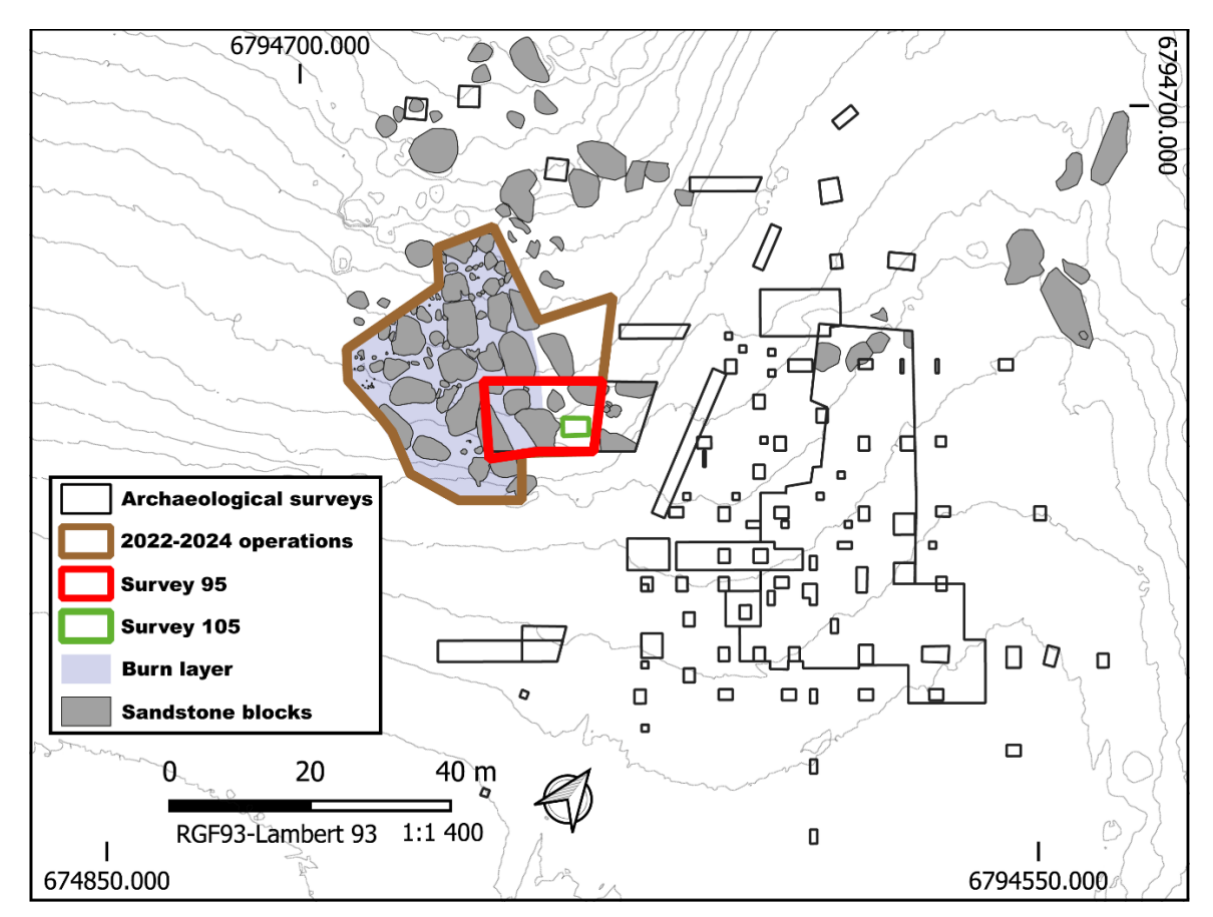


Fig. 1. Map of Ormesson, with the location of survey 95 indicated by a red rectangle (H.G. Naton and L. Heccan, modified by I. Notterpek).

The first occupation, characterised by Levallois point production, was present in the southeast corner of survey 95. Artefacts were found in local aeolian sands dated by optically stimulated luminescence (OSL) to 105.2 ± 5.5 ka (OSL 95-1) (Fig. 2). The second occupation, characterised by preferential Levallois reduction, was identified in the western half of survey 95 directly below extensive burned deposits ranging from 3 to 10 cm in thickness. The massive sandstone blocks were present and in their current tilted positions at the time of deposition. OSL dating of the layered aeolian sands above the burned layer yielded an age of 90.4 ± 6 ka (OSL 95-12), while the underlying geological substratum (Fontainebleau sand) provided an age of > 583 ka (OSL 95-11) (Fig. 2). Together, these results establish a *terminus ante quem* of approximately 90 ka for both the burned layer and the associated Levallois

occupation. These chronometric data place the burned deposits within the morpho-sedimentary framework of the Early Weichselian glacial period, broadly corresponding to Marine Isotope Stage 5 (MIS 5) (dosimetry details of all OSL dates are available in Table S1, sheet 1) (Müller et al., 2003; Helmens, 2014). However, the two Levallois occupations cannot be stratigraphically linked due to a major gully erosion phase that truncated the deposits, with infill sediments dated to $83.5 \pm 4.0 \, \text{ka}$ (OSL 95-10) (Fig. 2). Although the burned layer and associated Levallois occupation likely date between 90.4 $\pm 6 \, \text{ka}$ and $105.2 \pm 5.5 \, \text{ka}$, potentially aligning with MIS 5c, this truncation precludes secure correlation between the dated contexts. Accordingly, these deposits are assigned more generally to MIS 5.

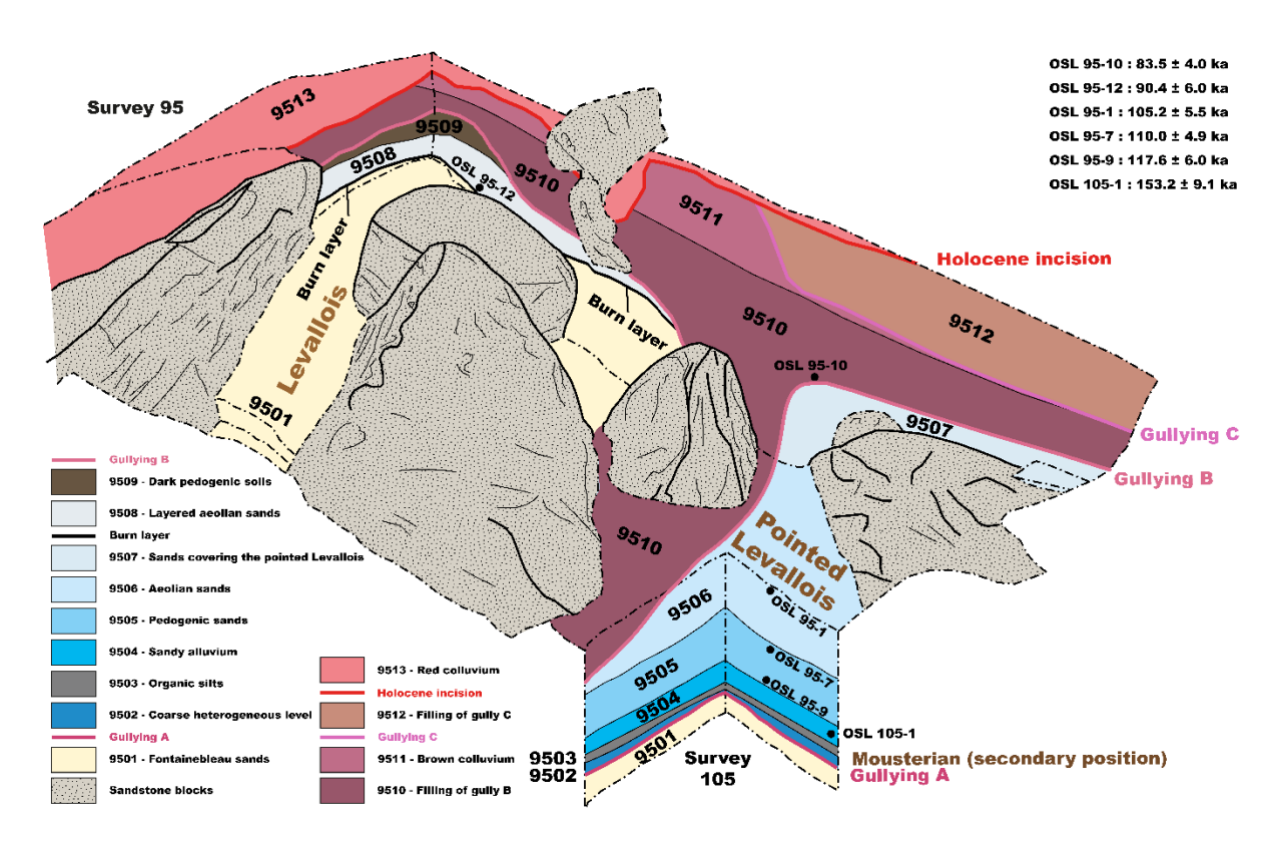


Fig. 2. Schematic drawing of surveys 95 and 105 with geological understandings, the location of optically stimulated luminescence samples, and their chronometric results (H.G. Naton, modified by I. Notterpek).

Extensions of the test pit have since revealed that the burned deposits are substantial, extending over approximately 700 m², and may represent no more than the relic of a much larger burned surface. However, at the time of discovery, only the burned deposits covering approximately 30 m² in survey 95 were known. In certain areas, several burned layers were also visible. These

combustion residues therefore required investigation, alongside an assessment of lipid biomarker and BPCA analyses as biomolecular approaches for characterising past fire traces.

3. Materials and methods

3.1. Charcoal samples for anthracological study

All soil from the burned layer(s) was systematically sieved to 2 mm, and burned material was randomly selected from the sieved material for anthracological study. The following units of survey 95 and the number of specimens studied were as follows, for a total of 119 burned fragments: I7 (n = 1), I8 (n = 33), I9 (n = 10), I10 (n = 11), I11 (n = 2), I12 (n = 20), I13 (n = 1), I14 (n = 1), I15 (n = 1), J11 (n = 1), L15 (n = 1), M15 (n = 1), and M17 (n = 15) (Fig. 3). The number of samples per square metre does not reflect the total number of charcoal fragments present, but rather the number selected for analysis through random sampling of the charcoal remains.

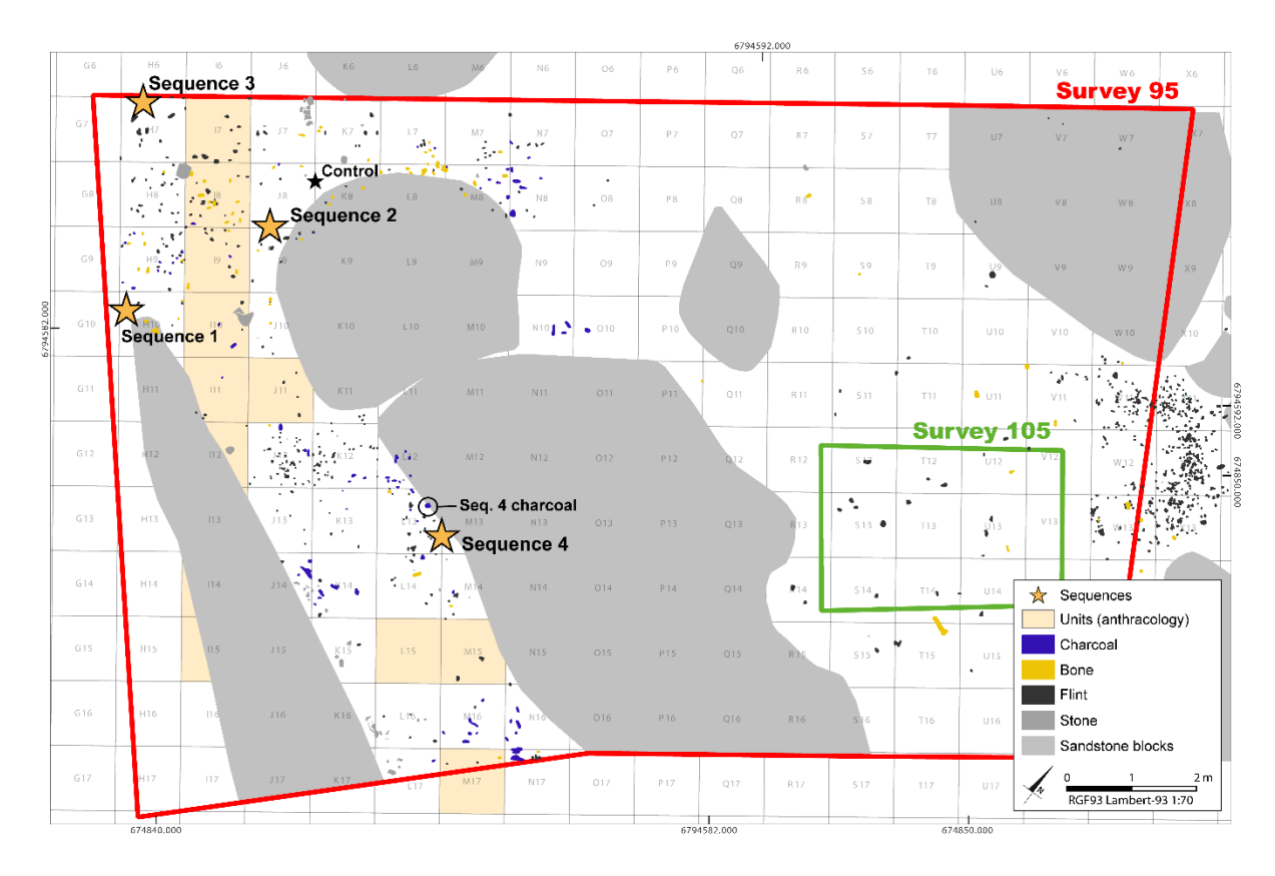


Fig. 3. Map of survey 95 with all sample locations. Units from which charcoal material were randomly selected for anthracological analysis are shaded in yellow. The location of soil sequences is indicated by a yellow star, and the control is indicated by a black star. The in-plan charcoal sample of sequence

4 is plotted and labelled. Archaeological material is shown with charcoal (blue), bone (yellow), flint (dark grey), and stone (grey).

3.2. Soil and charcoal samples for geochemical analyses

178

179

180

181

182

183

184

185

186

187

188

189

190

191

192

193

194

195

196

197

198

199

200

For organic geochemical and biomolecular analyses, four sequences of samples were taken from different areas of the burned deposits in survey 95. Each sequence consisted of at least 5 soil samples, collected from bottom to top, that were spaced approximately 2-5 cm apart depending on the area sampled. Sequence 1 was located in the southwestern profile of unit H10 (~77.813-77.964 metres above sea level), sequence 2 in the northern profile of unit J9 (~77.515-77.672 m a.s.l.), sequence 3 in the northern profile of unit H7 (~77.788–77.969 m a.s.l.), and sequence 4 in the eastern profile of unit M13 (~77.673–77.858 m a.s.l.) (Fig. 3). For each sequence, a macrocharcoal remain near the soil sampling zone with an estimated weight of least 10 mg was collected for BPCA analysis (C1-4). Each associated charcoal was sampled in profile (Fig. 4), with the exception of the fourth charcoal (C4). As no macrocharcoal fragments were visible in the profile of sequence 4, a large charcoal in the active excavation surface of unit L13 was collected (Figs 3 and 4). Adhering soil was carefully removed under sterile laboratory conditions and pure charcoal was collected for analysis. For sequence 2, a total of 6 rather than 5 soil samples were gathered. Sample J9 3b was collected at the same elevation of the associated charcoal (C2), but deeper in the profile (Fig. 4). It was retained as a separate sample given its high charcoal content, and was sampled prior to the true soil sample J9 3, again at the same elevation but deeper in the profile. The geological substratum (Fontainebleau sand) was collected as a sterile control in the eastern profile of unit J8, approximately 60 cm beneath the burned layer (77.246 m a.s.l.). Each sequence was photographed before, during, and after sampling, and the elevation of each sample was recorded with a Total Station. All samples were gathered using sterilised stainlesssteel tools and were stored in sterile glass tubes to avoid plastic contamination.

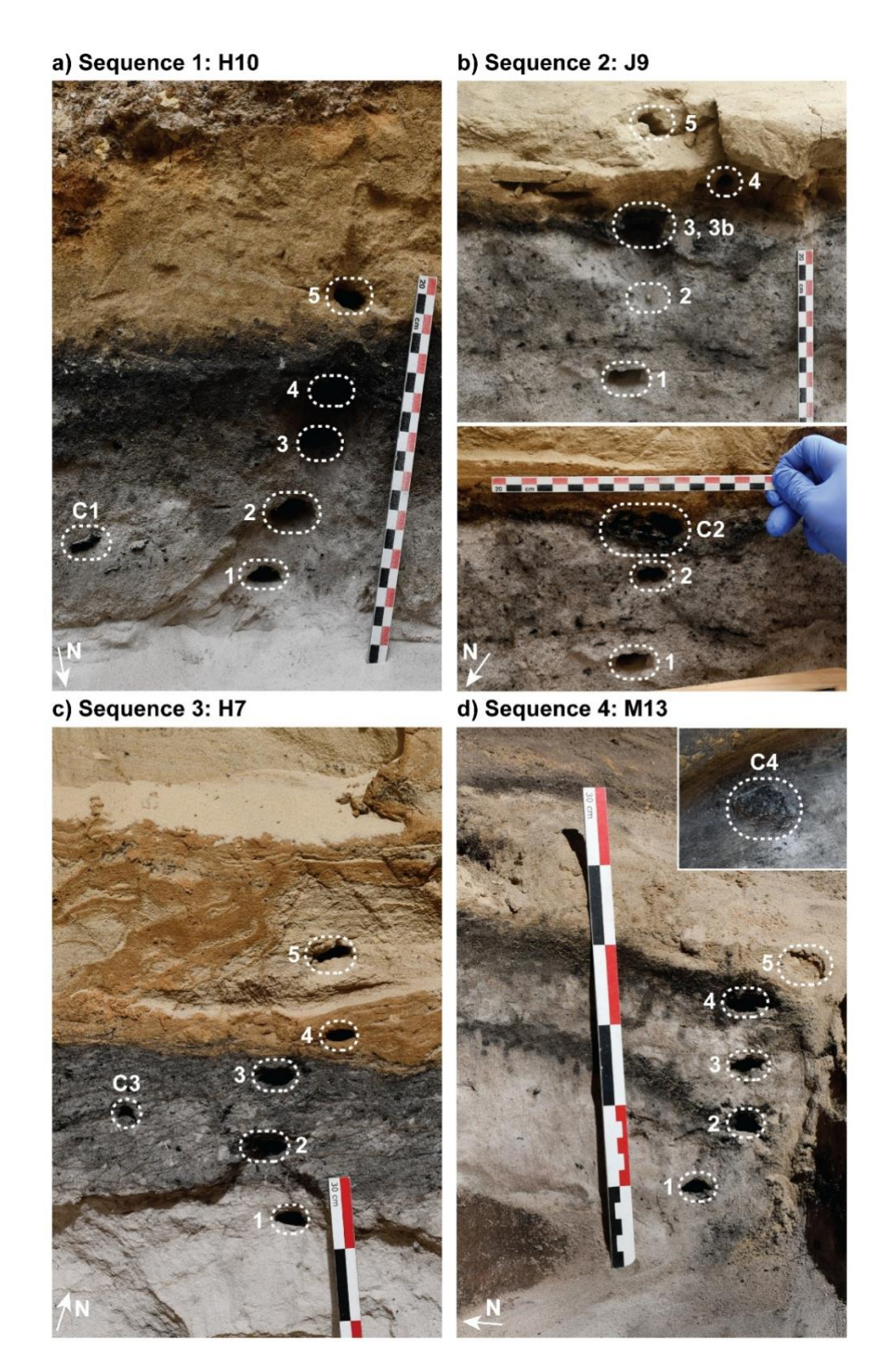


Fig. 4. Samples collected for geochemical analysis. Sequences 1–4, with the location of each sample indicated by a dashed white oval. The associated charcoal for each sequence (C1–4), here prior to sampling, is also shown. In b) sequence 2, the bottom image shows sample 2 and charcoal C2 prior to partial collapse of the profile. The inlay in d) sequence 4 shows charcoal C4 located on the excavation surface of unit L13.

3.3. Methods

Methods included anthracology, bulk elemental and stable isotope analyses, pH measurement, lipid extraction and analysis, and BPCA analysis. Anthracological study was performed on the 119 burned samples described in section 3.1, and the charcoal was studied with microscopy by classical botanical identification based on the three anatomical planes of wood (radial, transversal, tangential). Charcoal collected for geochemical analyses were not studied via anthracology to avoid contamination. Bulk elemental and stable isotope analyses were performed on all samples (n = 26), while pH measurement was performed only on the control soil. Lipid extraction and analysis was performed on soil samples (n = 22), while BPCA analysis was conducted on both soil and charcoal samples (n = 26). Full methodological details are relayed in the supplementary information (SI-1).

Briefly, lipids were extracted from soil samples to characterise OM composition using protocols for solvent extraction with dichloromethane and methanol (modified from Jambrina-Enríquez et al., 2019), and acid extraction using the one-step acidified methanol extraction described by Craig et al. (2013). Analysis of the total lipid extract (TLE) was performed by gas chromatography mass spectrometry (GC-MS). The NIST mass spectra library and MassHunter software (Agilent technologies) were used for compound identification and quantification. Lipid yields are reported as µg per gram dry sample (µg/gds), and the various proxies calculated to interpret aliphatic lipid data are relayed in Table 1. These proxies were mobilised to evaluate the contributions of various biogenic sources to SOM, as well as to characterise the preservation state of these compounds, including the detection of microbial reworking or modern lipid input.

Table 1. Summary of aliphatic lipid proxies with formulae, references, and the range of compounds utilised (where applicable).

Proxy	Equation	References, range of compounds
Average chain length (ACL)	$\frac{\sum C_i \times i}{\sum C_i}$, where C_i is the relative amount of n -aliphatic compound with i carbons	General: Poynter et al., 1989. n -Alkanes: C_{16} - C_{35} (this study), ACL_{long} : C_{27} - C_{33} odd (Schäfer et al., 2016). n -Alkanols: C_{22} - C_{28} (Zheng et al., 2009),

n -Alkanoic acids: $C_{12:0}$ - $C_{34:0}$, ACL_{long} :	
$C_{20:0}$ – $C_{34:0 \text{ even}}$ (this study).	

Carbon preference index (CPI) $\frac{(\Sigma_{i=n}^{m}C_{2i+1})+(\Sigma_{i=n+1}^{m+1}C_{2i+1})}{2(\Sigma_{i=n+1}^{m+1}C_{2i})}, \text{ where } n \text{ is the }$ $\frac{\text{General: Marzi et al., 1993.}}{n-\text{Alkanes: C}_{16}-\text{C}_{32}, \text{CPI}_{long: C}_{24}-\text{C}_{32}}$

starting n-aliphatic compound divided by 2 and m is the ending n-aliphatic compound divided by 2 (Knicker et al., 2013). n-Alkanois: C_{23} - C_{33} (Zhang et al., 2006). n-Alkanoic acids: $C_{10:0}$ - $C_{29:0}$ (Knicker et

al., 2013), CPI_{long}: C_{20:0}–C_{31:0} (Wiesenberg

et al., 2012).

n-Alkanes

$$rac{D_{31}+C_{33}}{C_{27}+C_{31}+C_{33}}$$
 Schäfer et al., 2016

Odd-over-even
$$\frac{C_{27}+C_{29}+C_{31}+C_{33}}{C_{26}+C_{28}+C_{30}+C_{32}}$$
 Hoefs et al., 2002

Ratio of short- to long-
$$\sum C_{16-24}$$
 after Buggle et al., 2010 chain (R_{S/I}) $\sum C_{25-33}$

n-Alkanols

Alkanol index
$$\frac{C_{30}}{C_{28}+C_{30}}$$
 Zhang et al., 2006

$$C_{24}/C_{26}$$
 Zheng et al., 2009

n-Alkanoic acids

230

231

232

233

Even-over-odd
$$C_{24}+C_{26}+C_{28}+C_{30}+C_{32}$$
 Schäfer et al., 2016 predominance (EOP) $C_{23}+C_{25}+C_{27}+C_{29}+C_{31}$

Ratio of short- to long-
$$\sum C_{10-20}$$
 Knicker et al., 2013 chain (FA_{s/l}) $\sum C_{21-28}$

Palmitic/stearic acid
$$\frac{C_{16:0}}{c_{16:0}}$$
 Eerkens, 2005

C18_{unsaturated/saturated}
$$C_{18:1} + C_{18:2} \over C_{18:0}$$
 Wiesenberg et al., 2012

Carbon diversity index
$$\frac{x}{C_{24}+C_{28}+C_{32}+C_{34}}$$
, where x is C_{24} (CDI-C), Schäfer et al., 2016 (CDI) C_{28} (CDI-D), and $C_{32}+C_{34}$ (CDI-G)

Lastly, BPCA analysis was conducted to quantify molecular PyC in soil and charcoal samples, providing information on the aromaticity and aromatic condensation of the charred residues. The procedure followed was that of Glaser et al. (1998) with the modifications of Brodowski et al. (2005), and analyses were performed by GC with flame ionisation detection (GC-FID). BPCA yields were

converted to black carbon or PyC contents using the 2.27 correction factor proposed by Glaser et al. (1998). Results are reported as g BPCA-C/kg dry sample, as well as normalised to sample TOC (g BPCA-C/kg OC). BPCA yields were further processed with the random forest algorithms of Notterpek et al. (2025) to predict HTT and precursor feedstock types (hardwoods, softwoods, grasses). Quantitative HTT uncertainties were calculated at 95% and 68% confidence intervals, with errors for averaged values reflecting the square root of the sum of variances.

4. Results

4.1. Anthracology: taxonomy and state of the wood

Anthracological analysis was conducted on a subsample of 119 burned fragments, of which 114 were charcoal, 4 were bone, and 1 was a seed pericarp. The charcoal assemblage was composed of Betula sp. (n = 7), Pinus cf. sylvestris/nigra (n = 100), gymnosperm (n = 3), and 4 unidentifiable fragments. Several anatomical signatures provide a more precise description of the state of the wood at the time of combustion (Théry-Parisot, 2001; Marguerie and Hunot, 2007; Théry-Parisot and Henry, 2012; Henry and Théry-Parisot, 2014; Vidal-Matutano et al., 2017, 2020). The most predominant characteristic observed was that of vitrification, present in 67% of the charcoal assemblage. Three levels of vitrification were observed: (i) low intensity, characterised by reflective patches with no alteration of the anatomical structure of the wood (Fig. 5a); (ii) intermediate intensity, wherein the anatomical structure was only observable in a small part of the sample (Fig. 5b); and (iii) high intensity, evincing a massive melting of the anatomical structure (Fig. 5c). Elsewhere, 48% of samples showed reaction wood characteristic of branches (Fig. 5d), 13% showed decay characteristic of dead wood (Fig. 5e), and 7% showed shrinkage cracks characteristic of green wood combustion (Fig. 5f).

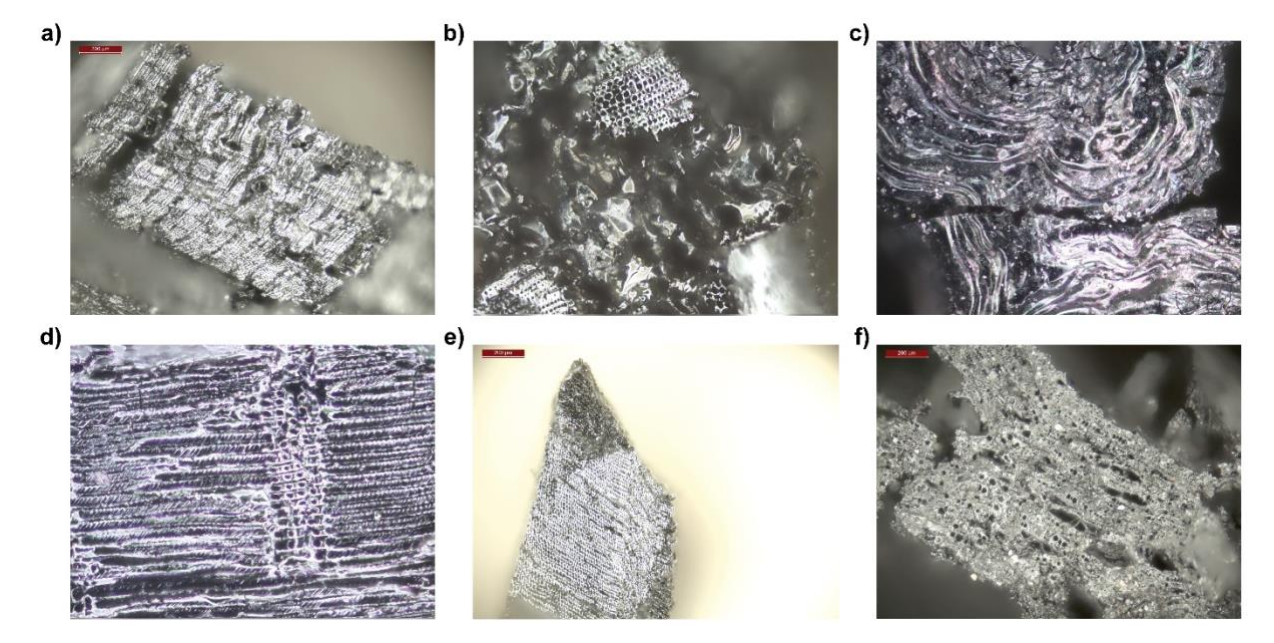


Fig. 5. Anatomical signatures identified in the charcoal assemblage. a) *Pinus* cf. *sylvestris/nigra* (transversal section x100), vitrification with preservation of the anatomical structure of the wood; b) *Pinus* cf. *sylvestris/nigra* (transversal section x100), patches with intense vitrification with the anatomical structure only observable in sections of the sample; c) unidentifiable vitrified sample (transversal section x100) with massive melting of the anatomical structure; d) *Pinus* cf. *sylvestris/nigra* (radial section x100), reaction wood characteristic of branches; e) *Pinus* cf. *sylvestris/nigra*, (radial section x100), dead wood with collapsed cell walls and major cellular deformations, type A.L. 3 (Henry and Théry-Parisot, 2014); f) *Betula* sp. (transversal section x100), wood with radial cracks characteristic of the combustion of green wood (Théry-Parisot and Henry, 2012).

4.2. Lipid biomarkers

Control pH and the bulk elemental and stable isotope results of soil and charcoal samples are relayed in the supplementary information (SI-1 and Table S1, sheet 2). The total lipid yields obtained by solvent and acid extraction are shown in Figure 6 (see also Table S1, sheet 3). The TLE obtained by solvent extraction yielded an average of $2.83 \pm 1.49 \, \mu g$ per gram dry sample (gds) for all samples, with contents ranging from 0.75 (H10 1) to 6.14 (J9 3b) $\mu g/gds$. Sample H7 1 is excluded from this description, as a large plasticiser peak in the silylated solvent extract obfuscated accurate quantification; henceforth, summary statistics for compounds quantified from the solvent extract exclude sample H7 1, while those for compounds quantified from the acidified methanol extract include all samples. The TLE obtained by acid extraction yielded an average of $8.59 \pm 6.75 \, \mu g/gds$, with the lowest concentration in the control (1.24 $\mu g/gds$) and the highest in sample M13 2 (32.82 $\mu g/gds$). Acid extraction yielded higher lipid contents for all samples, with the exceptions of the control (in

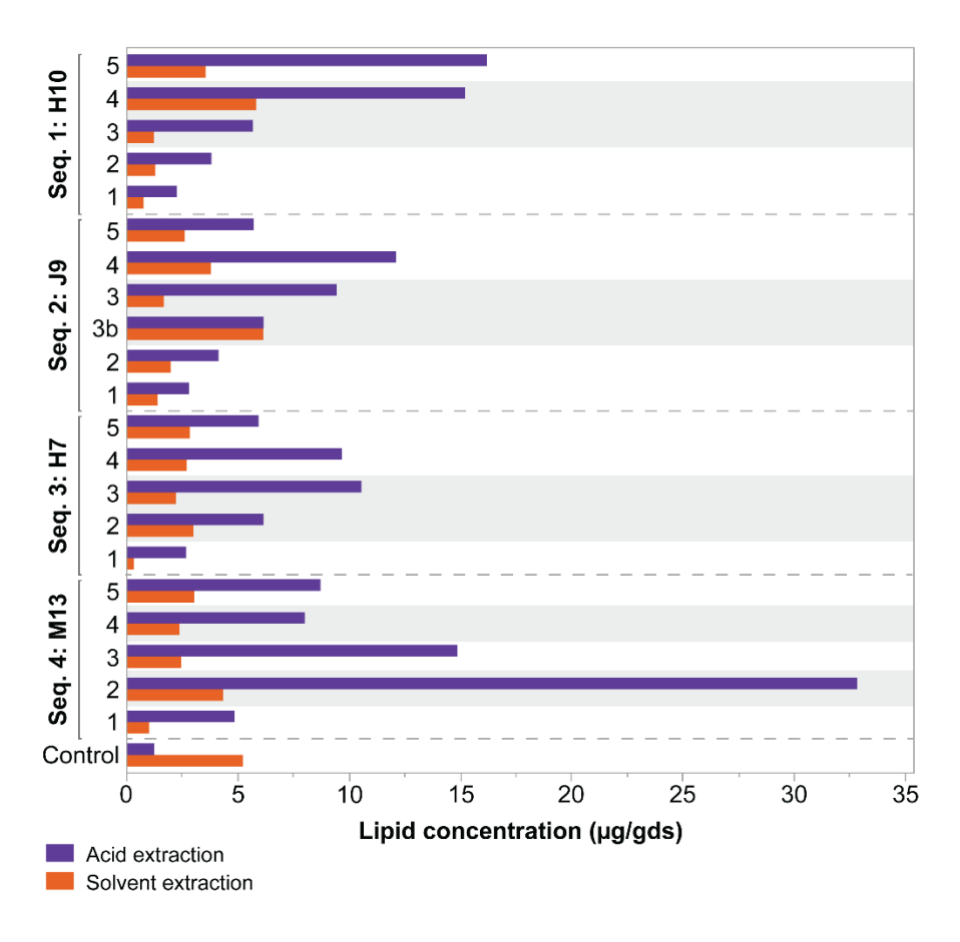


Fig. 6. Total lipid yields in microgram per gram of dry sample ($\mu g/gds$) obtained by acid and solvent extraction. The position of the burned layer(s) within each sequence is indicated by a shaded grey bar.

4.2.1. *n*-Alkanes

n-Alkanes ranging from C₁₆ to C₃₅ were identified and quantified in the TLE obtained by solvent extraction (Table S1, sheet 4). Long-chain (> C₂₉), odd-numbered n-alkanes were particularly prevalent in samples in and above the burned layer (Fig. S3). Total n-alkane yields (μ g/gds) ranged from 0.12 to 1.12 with an average of 0.48 \pm 0.29 μ g/gds for all samples (Fig. 7). The control yielded 0.59 μ g n-alkane/gds. n-alkane ACL values varied from 27.17 to 29.39, and ACL_{long} values from 29.36 to 30.65. When averaged according to sample stratigraphy, both ACL and ACL_{long} increased with ascending elevation on the order of 1.18 for ACL and 0.49 for ACL_{long} (values denote the difference in means between "below" and "above" samples among all sequences, with below samples excluding the control), though a slight dip is observed in the uppermost sample of sequences 2 and 3 (Fig. 7). n-

Alkane ratio values ranged from 0.53 to 0.87, and generally increased from samples below the burned layer (0.59 \pm 0.05) to those in (0.67 \pm 0.10) and above it (0.80 \pm 0.06) (Fig. 7). OEP values spanned from 0.79 to 5.01 and values of >3 were obtained for all samples above the burned layer, with the exception of sequence 4, which yielded values between 1 and 2 (Fig. 7). On average, OEP values thus increased from samples below the burned layer (1.14 \pm 0.10) to those above it (3.59 \pm 0.85). Results of the closely related CPI are relayed in the supplementary information (SI-1). Lastly, R_{S/I} values ranged from 0.09 to 0.44, with the highest average values obtained for samples below the burned layer (0.33 \pm 0.05) and the lowest for those above it (0.14 \pm 0.04) (Fig. 7).

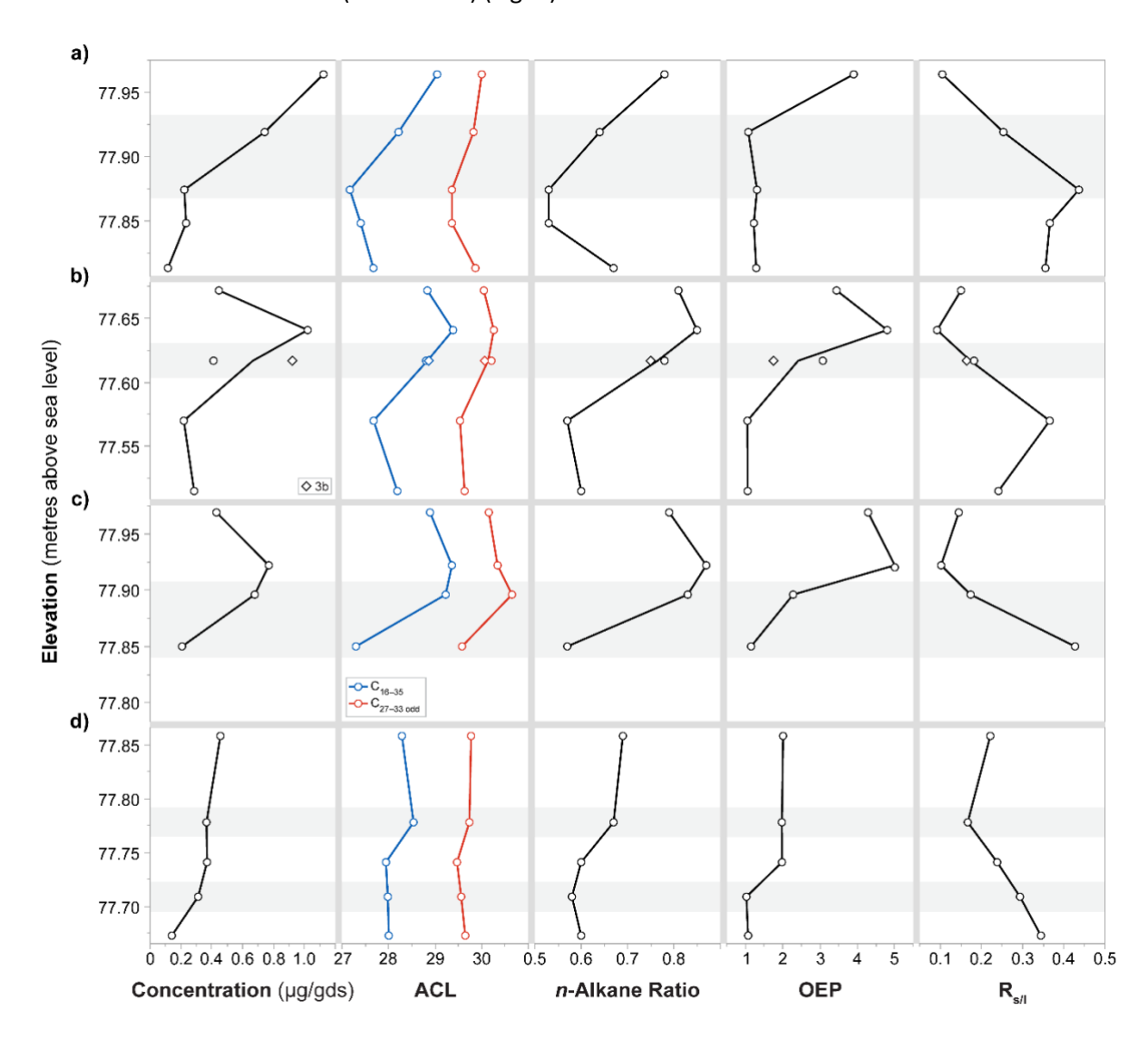


Fig. 7. Quantitative n-alkane results for sequences a) 1, b) 2, c) 3, and d) 4. From left to right: (i) concentration (μ g/gds), (ii) ACL (blue) and ACL_{long} (red), (iii) n-alkane ratio, (iv) OEP, and (v) R_{s/l}. The position of the burned layer(s) within each sequence is indicated by a shaded grey bar. Sample H7 1 is omitted, and the charcoal-rich sample J9 3b is denoted by a diamond.

4.2.2. *n*-Alkanols

n-Alkanols ranging from 12 to 34 carbons were identified and quantified in the TLE obtained by solvent extraction (Table S1, sheet 5), with the exception of C_{17} and C_{19} as these compounds were too close in retention time to $C_{16:0}$ and $C_{18:0}$ n-alkanoic acids to be accurately quantified. The recovered n-alkanols were predominantly of even-numbered carbon chain length, and as for n-alkanes, long-chain n-alkanols (> C_{24}) were more abundant in samples in and above the burned layer (Fig. S4). C_{18} was particularly abundant in the control (~48%) (Table S1, sheet 5). The ACL of n-alkanols (C_{22} - C_{28}) ranged from 23.52 to 26.11, with average values of 24.28 \pm 0.26 in samples below the burned layer and 25.83 \pm 0.25 in those above it (Fig. 8). The ACL of long-chain, even-numbered n-alkanols ($C_{24-32\,\text{even}}$) also generally increased from samples below (26.69 \pm 0.47) to above (27.43 \pm 0.25) the burned layer (Fig. 8). The alkanol index yielded values ranging from 0.30 to 0.54, with average values of 0.32 \pm 0.01 in samples below the burned layer and 0.46 \pm 0.02 in samples above it (Fig. 8). Lastly, C_{24}/C_{26} produced values spanning between 0.22 and 2.25, with the highest average values in samples below the burned layer (1.20 \pm 0.31) and the smallest in those above it (0.30 \pm 0.11) (Fig. 8). n-Alkanol CPI results are relayed in the supplementary information (SI-1).

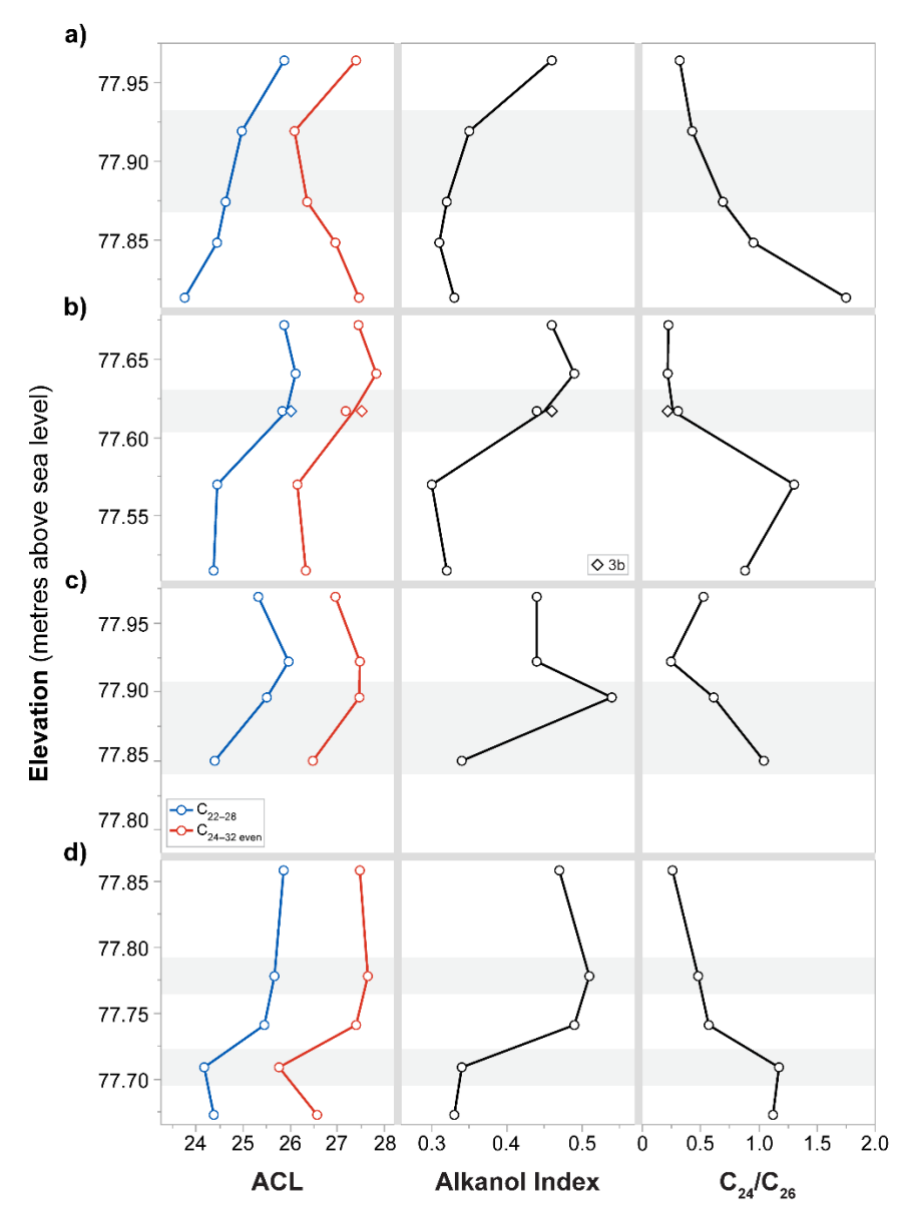


Fig. 8. *n*-Alkanol proxy results for sequences a) 1, b) 2, c) 3, and d) 4. From left to right: (i) ACL C_{22} – C_{28} (blue) and C_{24} – C_{32} even (red), (ii) alkanol index, and (iii) C_{24} / C_{26} . The position of the burned layer(s) within each sequence is indicated by a shaded grey bar. Sample H7 1 is omitted, and the charcoal-rich sample J9 3b is denoted by a diamond.

4.2.3. Saturated and unsaturated fatty acids

n-Alkanoic acids or saturated fatty acids (SFAs) ranging from 8 to 34 carbons were identified and quantified in acid-extracted samples (Table S1, sheet 6). Palmitic ($C_{16:0}$) and stearic ($C_{18:0}$) acid were the most dominant SFAs in all samples, and their relative contributions were more significant in samples below the burned layer, while samples situated in and above the burned layer generally yielded greater relative proportions of medium- to long-chain SFAs (Fig. S5). The unsaturated fatty acid $C_{16:1}$ was identified in 5 samples, $C_{18:1}$ in all 22 samples, and $C_{18:2}$ in 10 samples; $C_{18:3}$ was not identified

in any samples (Table S1, sheet 6). Lastly, two monoacylglycerols (monopalmitin and monostearin) were identified in several samples (Table S1, sheet 7).

Fatty acid ACL values varied from 17.42 to 23.70 with an average of 20.75 ± 1.75 for all samples, while those of ACL_{long} varied from 22.64 to 26.19 with an average of 25.02 ± 0.98 for all samples. The values yielded by these proxies generally increased with ascending elevation, on the order of 3.53 for ACL and 1.70 for ACL_{long} (values denote the difference in means), though a slight dip is similarly observed in the uppermost sample of sequences 2 and 3 (Fig. 9). EOP values ranged from 2.08 to 5.37 with an average of 2.89 ± 0.75 for all samples, and generally decreased from samples below the burned layer (3.43 \pm 0.46) to those in (2.56 \pm 0.23) and above it (2.45 \pm 0.18) (Fig. 9). Fatty acid CPI results are reported in the supplementary information (SI-1). FA_{s/l} values spanned from 0.75 to 108.46, and their average falls to 2.34 ± 1.72 when the high outlier of the control is removed. FA_{s/l} values were highest in samples below the burned layer (4.27 \pm 1.87), particularly in sequence 2, and generally decreased with ascending elevation to samples above the burned layer (average: 1.11 \pm 0.31) (Fig. 9). The ratio of C_{16:0}/C_{18:0} ranged from 0.51 to 1.05 (average: 0.74 \pm 0.14), with the highest values observed in samples from the burned layer (0.80 \pm 0.14). Lastly, C18_{unsat/sat} yielded values ranging from 0.002 to 0.71 (average: 0.18 \pm 0.14), which were once more highest in samples from burned layer (0.21 \pm 0.20) (Fig. 9).

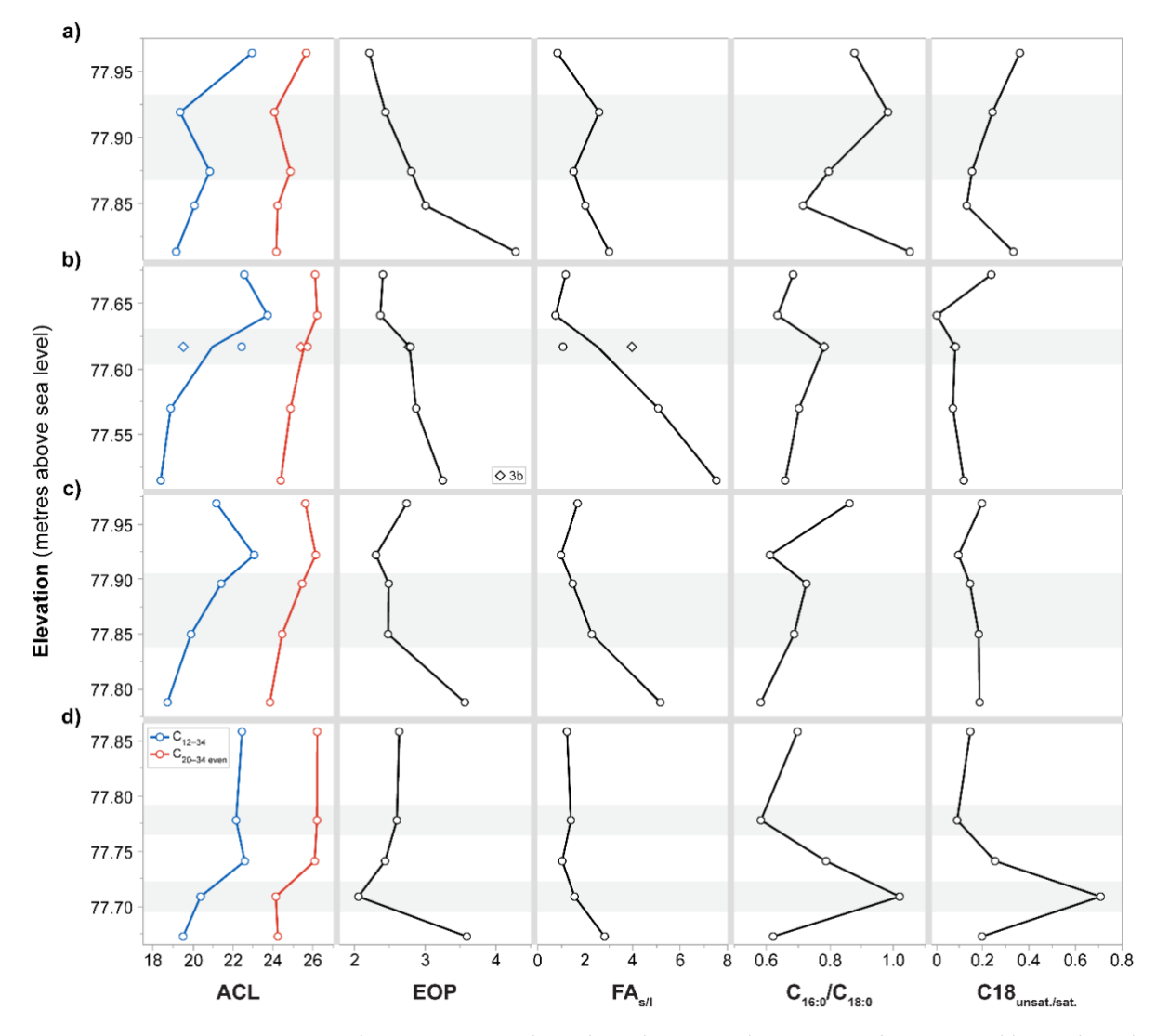


Fig. 9. Fatty acid proxy results for sequences a) 1, b) 2, c) 3, and d) 4. From left to right: (i) ACL (blue) and ACL_{long} (red), (ii) EOP, (iii) FA_{s/l}, (iv) $C_{16:0}/C_{18:0}$, and (v) C18_{unsat./sat.}. The position of the burned layer(s) within each sequence is indicated by a shaded grey bar. The charcoal-rich sample J9 3b is denoted by a diamond.

The CDI of Schäfer et al. (2016) was calculated to assess contributions of coniferous (CDI-C), deciduous (CDI-D), and grass (CDI-G) vegetation to saturated fatty acids, with values compiled in a ternary plot. As Figure 10 illustrates, the control and samples below the burned layer clustered around CDI-C values of approximately 0.74, CDI-D values of ~0.22, and CDI-G values of ~0.04. Two outliers (samples 1–2 of sequence 2) yielded lower CDI-C (~0.58), higher CDI-D (~0.31), and higher CDI-G (~0.12) values. Burned-layer samples were more variable: four fell within the range of aforementioned control/below values, while four others clustered with samples above the burned layer (Fig. 10).

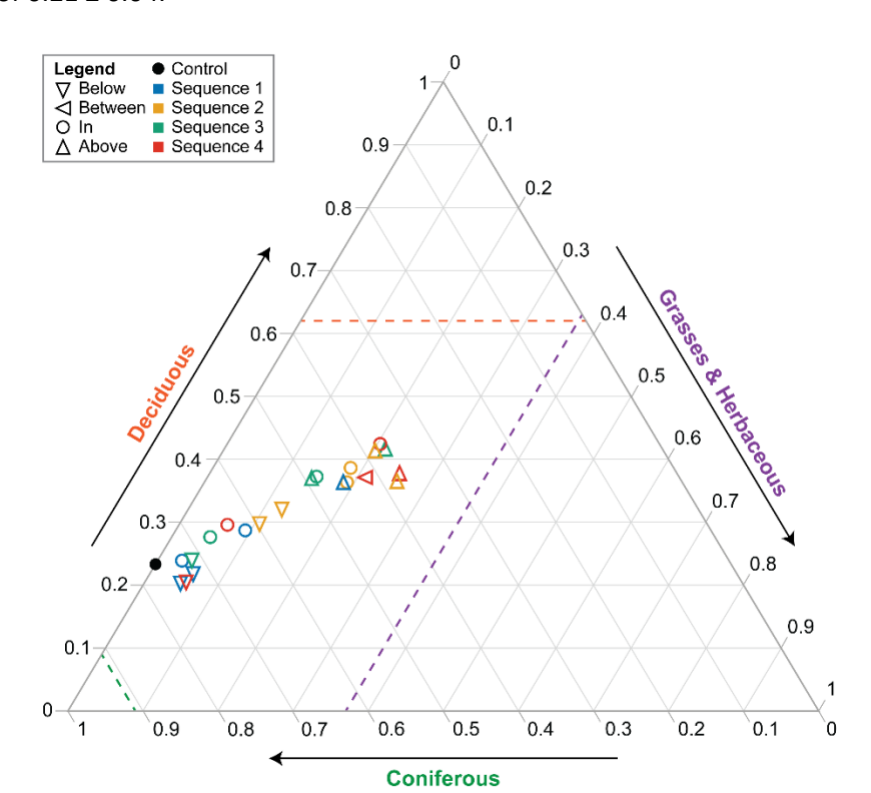


Fig. 10. Ternary plot of the Carbon Diversity Index. Samples are colour coded by sequence, with symbol shapes designating the stratigraphic position of the sample in relation to the burned layer(s). Reference lines are shown for each vegetation type with the maximum values (litter and topsoil) documented in the study of Schäfer et al. (2016).

4.2.4. Phytosterols and terpenoids

The TLE obtained by both solvent and acid extraction yielded various phytosterols and terpenoids (Table S1, sheet 7). A total of eight phytosterols were observed in both the solvent and acid extracts, and include compounds such as stigmast-5-ene, stigmasta-3,5-diene, stigmastanol, stigmasterol, β - and γ - sitosterol, and γ -sitostenone. Four diterpenoids were confidently identified in the solvent extract and include abietic acid, dehydroabietic acid, isopimaric acid, and methyl dehydroabietate. Numerous pentacyclic triterpenoids were also identified in both solvent and acid extracts, including: α - and β - amyrin, olean-13(18)-ene, friedelan-3-one, and D:A-friedoolean-6-ene, lupeol, lupenone, lupa-20,20(29)-dien-28-ol, betulone, betulinic acid, and betulin. Lupane family compounds (including betulin, betulone, and betulinic acid) were particularly abundant in sample M13 2, with only small or trace amounts in other samples. Other identified compounds indicative of plant

sources include a dialkyl ketone (nonacosan-10-one), a hopane, and wax esters of palmitic and stearic acids.

4.2.5. Aromatic biomarkers and selective ion monitoring results

379

380

381

382

383

384

385

386

387

388

389

390

391

392

393

394

395

396

397

398

399

400

401

402

Numerous aromatic hydrocarbons were identified in the solvent and acid extracts (Table S1, sheet 7). These included relatively simple compounds such as benzoic acid (and derivatives) and phthalic acid (derivatives and esters), as well as more complex compounds such as 7-oxo-7Hbenzocycloheptene-6,8-dicarboxylic acid and oxirane (2,2'-[(1-methylethylidene)-bis(4,1phenyleneoxymethylene)]bis). All benzene tricarboxylic acids (hemimellitic, trimellitic, and trimesic acid), tetracarboxylic acids (prehnitic, mellophanic, and pyromellitic acid), and possibly benzenepentacarboxylic acid were identified in the acid extracts of numerous samples. Interestingly, 2,4,6-hydroxy-trimesic acid was identified in a large number of samples. Several classes of PAHs and their derivatives were present, including: naphthalene (e.g., 2,6-naphthalenedicarboxylic acid), phenanthrene (e.g., 4-phenanthrene carboxylic acid, tetrahydroretene), and pyrene. An oxaspiro compound [7,9-di-tert-butyl-1-oxaspiro(4,5)deca-6,9-diene-2,8-dione] and two phenolic compounds [phenol, 2,4-bis(1,1-dimethylethyl)-, phosphite (3:1) and tris(2,4-ditert-butylphenyl)phosphate] were also identified in the majority of samples (see Table S1, sheet 7).

Selective ion monitoring (SIM) was also conducted to target four compound groups of interest: (i) trimethyltridecanoic acids (TMTD), (ii) phytanic acid, (iii) pristanic acid, and (iv) ω -(o-alkylphenyl)alkanoic acids (APAAs) (see supplementary information). TMTD and pristanic acids were not identified in any sample. Trace amounts of phytanic acid isomers (SRR and RRR) were identified in all samples (excluding the control) and the relative abundance of these isomers was very similar, suggesting possible bacterial origins. Trace amounts of C18 APAAs, namely the E and F isomers (Hansel et al., 2004; Evershed et al., 2008; Bondetti et al., 2021), were identified in a number of samples and were particularly clear in sample H7 2.

4.2.6. Diacids and hydroxy fatty acids

A wide range of dicarboxylic acids (diacids) and hydroxy (α -, β -, ω -) fatty acids were identified in the TLE obtained by acid extraction, and to a lesser extent solvent extraction. Diacids of 8 to 32 carbons were identified, and their relative distribution follows a similar pattern to that observed in other aliphatic compounds, wherein longer chain homologues are more prevalent in samples above the burned layer (Fig. S6, see also Table S1, sheet 8). α -Hydroxy fatty acids of 16 to 30 carbons, even-numbered ω -hydroxy fatty acids of 12 to 24 carbons, and numerous β -hydroxy fatty acids were also identified (Table S1, sheet 7).

4.3. Benzene polycarboxylic acids and random forest predictions

BPCA data was obtained for a total of 25 samples, as 1 sample (H10 1) did not yield any BPCAs (Table S1, sheet 9). The total BPCA contents of soil samples normalised to the weight of the sample (g BPCA-C/kg sample) ranged from 0.002 to 36.73 (average: 4.28 ± 8.58), while those of charcoal ranged from 28.53 to 146.46 (average: 62.10 ± 48.88). Total BPCA contents normalised to sample TOC (g BPCA-C/kg OC), which reflect PyC aromaticity, varied from 2.91 to 362.44 in soil samples (average: 175.48 \pm 127.79) and from 147.35 to 443.14 in charcoal (average: 290.26 \pm 118.96). The control yielded 0.003 g BPCA-C/kg sample or 2.94 g BPCA-C/kg OC, composed entirely of B3CA isomers (trimellitic and trimesic acid). Aromatic condensation values, reflected by the relative abundance of mellitic acid (B6CA% or BPCA_{cond}), ranged from 0 to 33.69 in soil samples (average: 14.65 \pm 13.00) and from 20.57 to 29.24 in charcoal (average: 23.84 \pm 3.31).

In sequence 1, total BPCA contents (g BPCA-C/kg OC) increased steadily from 161.92 in sample 2 to 291.88 in sample 4, and fell slightly to 270.60 in sample 5 (Fig. 11a). The relative distribution of BPCAs was quite consistent across soil samples, with an average of $8.80 \pm 0.8\%$ B3CA, $32.43 \pm 3.67\%$ B4CA, $35.43 \pm 0.88\%$ B5CA, and $23.35 \pm 4.44\%$ B6CA. The associated charcoal (C1) yielded 443.14 g BPCA-C/kg OC, of which 29.24% were B6CA. Sequence 2 BPCA contents were highest in the burned layer (samples 3 and 3b, average: 353.7 ± 8.74), and decreased by approximately 250 g BPCA-C/kg OC to samples 2 and 4 (Fig. 11b). B6CA contents were significantly higher in samples 3 and 3b (29.87 \pm

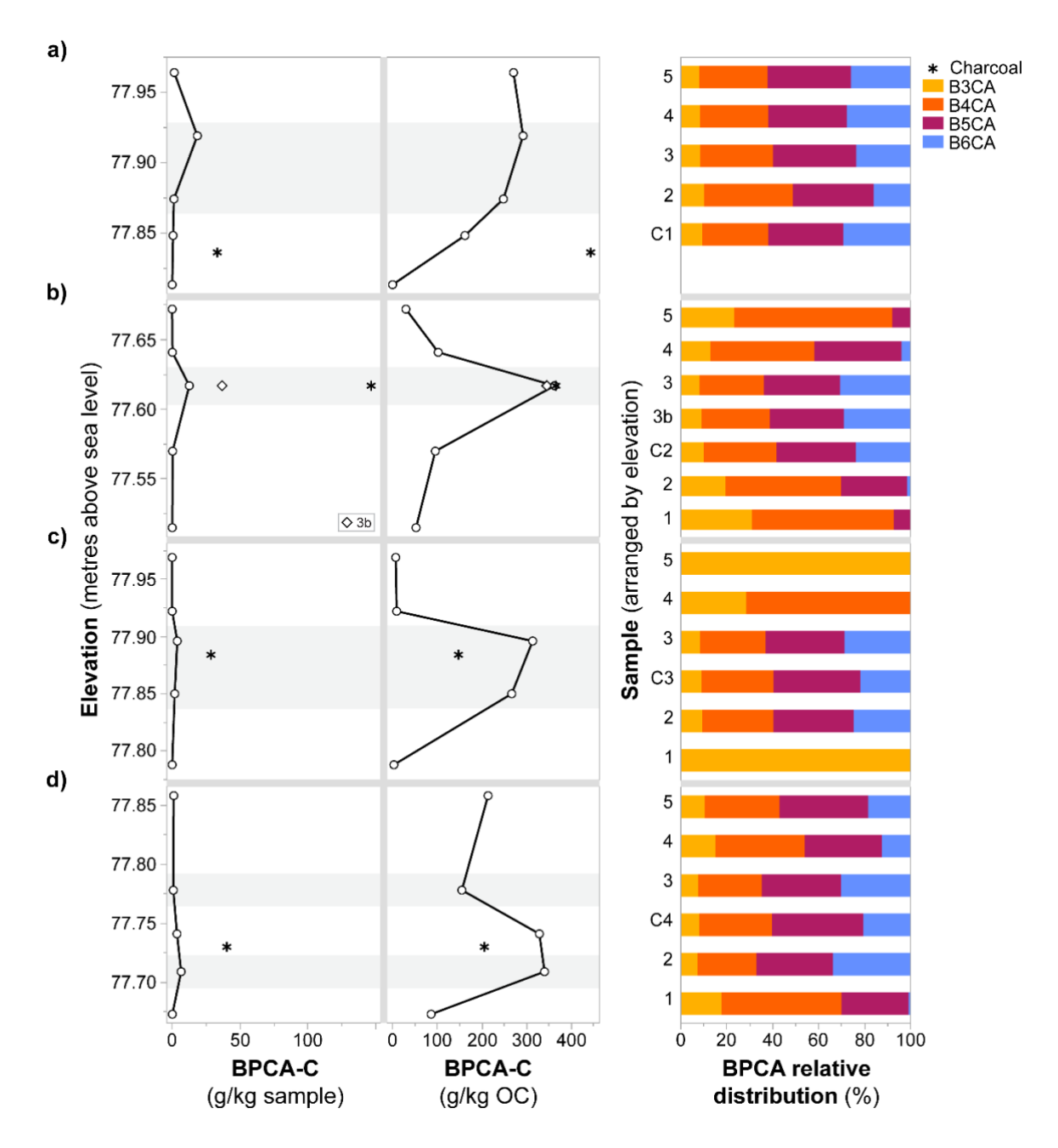


Fig. 11. BPCA results of sequences a) 1, b) 2, c) 3, and d) 4. From left to right: (i) total BPCA-C contents normalised to sample weight (g BPCA-C/kg sample), (ii) total BPCA-C contents normalised to TOC (g BPCA-C/kg OC), and (iii) the relative distribution of BPCAs containing 3–6 carboxylic acid substitutions. The position of the burned layer(s) within each sequence is indicated by a shaded grey bar. The charcoal-rich sample J9 3b is denoted by a diamond, and charcoal samples are denoted by an asterisk (*).

In sequence 3, samples 1 and 5 had the lowest BPCA contents (2.91 and 7.01 g BPCA-C/kg OC, respectively), which were composed exclusively of the B3CA isomer trimesic acid (Fig. 11c). Sample 4 yielded the third lowest BPCA content (9.18 g BPCA-C/kg OC), composed of only B3CAs and B4CAs. The full suite of BPCAs were present in samples 2 and 3, and sample 3 contained both a larger amount of BPCAs (313.38 g BPCA-C/kg OC) and a higher proportion of B6CA (28.73%) than sample 2. The associated charcoal (C3) yielded lower BPCA contents (147.35 g BPCA-C/kg OC) and a lower proportion of B6CA (21.85%) than soil samples located in the burned layer. Sequence 4 was unique in that two burned layers were visible in profile (samples 2 and 4), separated by seemingly unburned deposits (samples 1, 3, and 5). The lower burned layer (sample 2) produced the highest BPCA content in this sequence (339.88 g BPCA-C/kg OC) and the highest B6CA proportion (33.69%) of all samples analysed (Fig. 11d). Values declined slightly in the intervening deposit (sample 3: 328.39 g BPCA-C/kg, 30.33% B6CA) and more substantially in the upper burned layer (sample 4: 155.04 g BPCA-C/kg OC, 12.45% B6CA), before rising again in sample 5 (213.66 g BPCA-C/kg OC, 18.44% B6CA). Sample 1 yielded the lowest values of the sequence, with 86.27 g BPCA-C/kg OC and only 0.76% B6CA. The charcoal recovered in plan (C4) contained 205.40 g BPCA-C/kg OC, of which 20.57% were B6CA.

Quantitative and qualitative HTT predictions were obtained from BPCA results for the 19 samples that yielded B3CA–B6CA (Table S1, sheet 9). At 95% confidence, soil HTT estimates ranged from 159 ± 106 °C to 564 ± 164 °C, with an overall average of 361 ± 172 °C (n = 15). Samples from the burned layer produced a higher average of 419 ± 190 °C, which narrowed to 413 ± 98 °C at 68% confidence. These quantitative results are consistent with qualitative probability distributions. For example, while all soil samples were most frequently assigned to the 200-400 °C temperature class (0.60 ± 0.20) , burned-layer samples showed higher probabilities of assignment to the 400-600 °C class (0.20 ± 0.08) compared to samples below (0.03 ± 0.02) or above (0.04 ± 0.02) the burned layer (Fig. 12). The four charcoal samples produced HTT estimates ranging from 311 ± 152 to 389 ± 161 °C, with an average of 355 ± 146 °C that is narrowed to 358 ± 84 °C at 68% confidence. Charcoal samples were similarly most frequently assigned to the 200-400 °C temperature class (0.76 ± 0.06) . Regarding

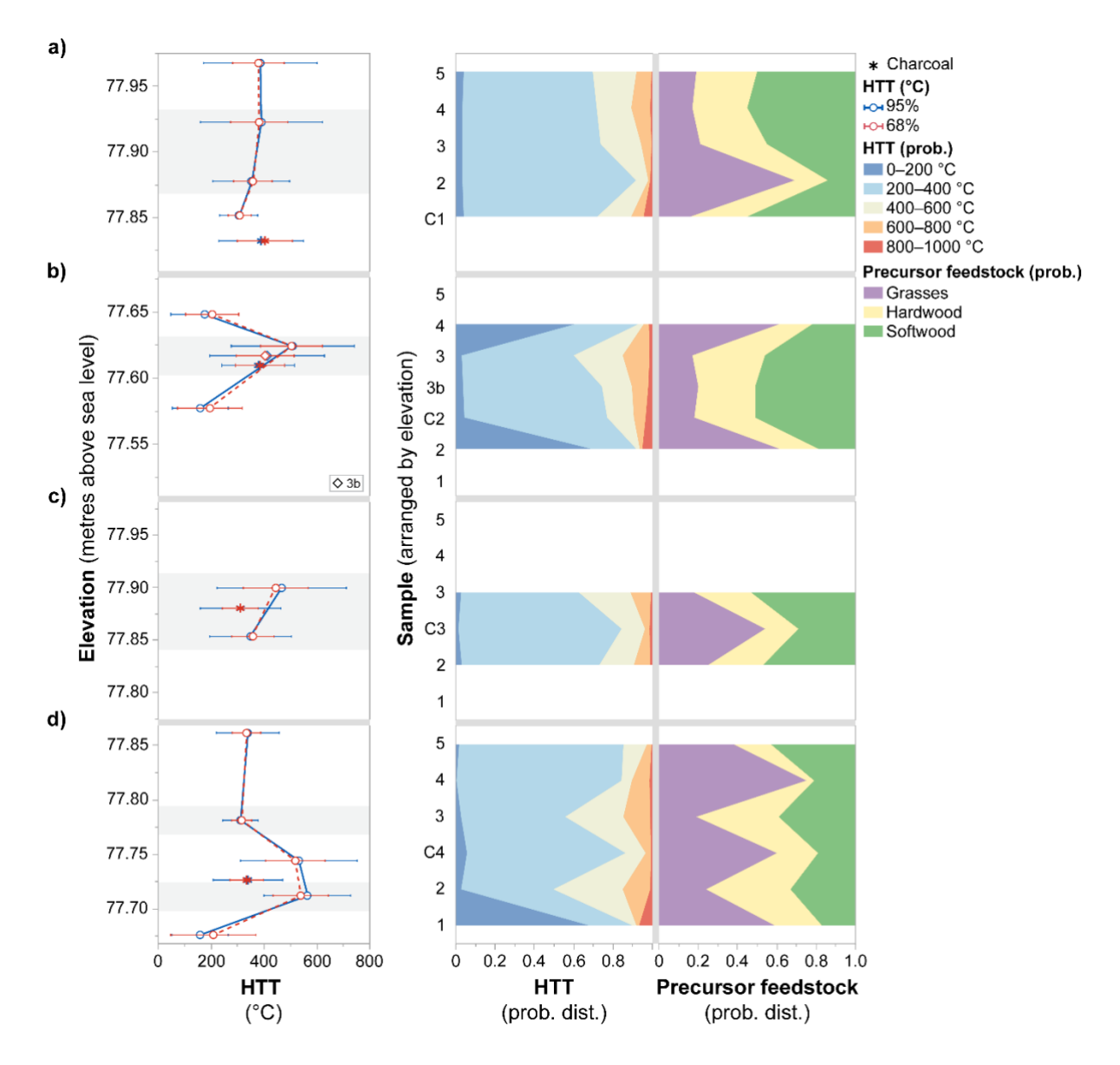


Fig. 12. Random forest predictions of heat treatment temperature (HTT, °C) and precursor feedstock (PF) category for sequences a) 1, b) 2, c) 3, and d) 4. From left to right: (i) quantitative predictions of HTT (°C) with confidence intervals of 68% (red) and 95% (blue), (ii) qualitative predictions (probability distribution) of HTT (°C) in 200 °C increments, where each range is exclusive of the minimum and inclusive of the maximum value; and (ii) qualitative predictions (probability distribution) of precursor feedstock at the level of grasses (purple), hardwoods (yellow), and softwoods (green). The position of the burned layer(s) within each sequence is indicated by a shaded grey bar. The charcoal-rich sample J9 3b is denoted by a diamond, and charcoal samples are denoted by an asterisk (*).

In sequence 1, soil HTT predictions peaked in sample 4 with values of 391 \pm 231 °C (95%) and 382 \pm 108 °C (68%), though mean estimates for samples 3 and 5 were within 50 °C of these values (Fig.

12a). Charcoal C1 demonstrated high coherence with the soil estimates, and yielded the highest HTT of all charcoal samples (95%: 389 \pm 161 °C, 68%: 404 \pm 104 °C). Sequence 2 HTT predictions were highest in sample 3 (95%: 509 \pm 233 °C, 68%: 504 \pm 117 °C), followed by the charcoal-rich sample 3b (95%: 412 \pm 217 °C, 68%: 405 \pm 110 °C), and decreased substantially in samples 2 and 4 (Fig. 12b). Charcoal C2 produced the second highest HTT among charcoal samples (95%: 379 \pm 137 °C, 68%: 385 \pm 93 °C), albeit lower than soil estimates from the burned layer. Sequence 3 soil HTT values were limited to the two burned-layer samples and were higher in sample 3 (95%: 467 \pm 245 °C, 68%: 445 \pm 123 °C) than in sample 2 (95%: 350 \pm 154 °C, 68%: 358 \pm 80 °C) (Fig. 12c). Charcoal C3 yielded the lowest HTT of all charcoal samples (95%: 311 \pm 152 °C, 68%: 310 \pm 68 °C). In sequence 4, soil HTT was highest in sample 2, which produced the maximum of all samples at 564 \pm 164 °C (95%) and 539 \pm 105 °C (68%). Sample 3 predictions also exceeded 500 °C (95%: 532 \pm 220 °C, 68%: 518 \pm 112 °C), and these estimates decreased to approximately 300–350 °C in samples 4 and 5 (Fig. 12d). Associated charcoal C4 had the second lowest HTT of charcoal samples at 340 \pm 131 °C (95%) and 335 \pm 63 °C (68%).

5. Discussion

5.1. Post-depositional modifications to the study area and studied residues

The Fontainebleau sands in which the burned deposits at Ormesson were preserved are coarse, porous, and exhibit weak aggregate stability, likely due to the presence of microcrystalline quartz and amorphous silica (French and Worden, 2013). These characteristics favour erosion, as exemplified by gully B, which separated the two Levallois occupations (Fig. 2). Combustion residues were nevertheless preserved in the western portion of survey 95, likely due to a combination of both macro-scale geomorphological factors (e.g., physical protection against erosion by the large sandstone boulders) and finer-scale taphonomic processes that ultimately promoted the persistence of OM and PyC in these deposits, but must be taken into account for the reconstruction of these fire traces.

5.1.1. Pyrogenic carbon preservation

502

503

504

505

506

507

508

509

510

511

512

513

514

515

516

517

518

519

520

521

522

523

524

525

526

527

Post-depositional modifications affecting PyC preservation and their relevance to BPCA results are discussed in depth in Notterpek et al. (2025) (see also Vaezzadeh et al., 2023). The most prevalent taphonomic pathways influencing PyC preservation in survey 95 include fragmentation and movement, the extent of which depend upon characteristics of the depositional environment (e.g., soil type, aggregate stability), as well as PyC physical properties (e.g., precursor feedstock type, particle size, surface area) and pyrolysis parameters (e.g., HTT) (Knicker, 2011; Singh et al., 2012; Chrzazvez et al., 2014; Pignatello et al., 2015; Saiz et al., 2018; Bellè et al., 2021). The high porosity and low aggregate stability of Fontainebleau sands facilitate PyC export (e.g., via water erosion, infiltration) compared to finer soils with strong aggregation (Brodowski et al., 2006; Chang et al., 2020; Bellè et al., 2021). Thermal exposure can alter these properties, particularly when followed by rainfall (Certini, 2005; Shakesby, 2011; Moody et al., 2013; Abney and Berhe, 2018), with variable outcomes including heat-induced aggregate breakdown (Jian et al., 2018) or the wash-in of ash/PyC resulting in pore clogging and surface sealing (though this is less common in coarse sands; see Onda et al., 2008; Stoof et al., 2016). PyC turnover is also slower in quartz sands than in fresh soils (Singh et al., 2012), possibly due to the strong sorption affinity of PyC for mineral phases and the mobilisation of mineral-associated OM (Glaser et al., 2000; Schiedung et al., 2020), as well as the greater abundance of non-pyrogenic OM primers (Hamer et al., 2004) that stimulate microbial activity in pedogenic soils (Czimczik and Masiello, 2007).

While lateral displacement of PyC was minimal in protected areas (i.e., the western portion where combustion residues were preserved), vertical movement is evident in the displacement of macrocharcoal fragments (e.g., C1) and in the dissolution of the burned layer with depth (e.g., sequence 3) (Fig. 4). The gradual tapering of BPCA concentrations below the burned layer, particularly when normalised to TOC (e.g., sequences 1 and 2, Fig. 11), provides molecular evidence for the downward infiltration of particulate PyC. In sequence 1, the high BPCA contents (g BPCA-C/kg OC) of sample 5 indicate upward migration of PyC, plausibly via the floating of porous microcharcoal particles

given their high initial hydrophobicity (Rumpel et al., 2015; Abney and Berhe, 2018), though alternative mechanisms such as micro- and meso-faunal bioturbation may also play a role. Within sequence 4, BPCA contents and BPCA_{cond} values fluctuated in a manner unobserved for sequences 1–3. This variability most plausibly reflects localised post-depositional reworking linked to the adjacent sandstone boulder (Fig. 2). The high aromaticity and aromatic condensation of sample 2 (which taper toward sample 4) suggest that the first burned layer best represents the original burn deposit, with post-fire infilling creating a diluted upper layer (sample 4) that was consequently more exposed to taphonomic alteration. Field observations document heterogenous and mottled deposits in this zone, consistent with small-scale infilling.

528

529

530

531

532

533

534

535

536

537

538

539

540

541

542

543

544

545

546

547

548

549

550

551

552

Molecularly, dissolved or non-mineral-protected PyC is more susceptible to diagenetic processes (e.g., oxidation, leaching, and biodegradation) that may preferentially degrade less aromatic and more weakly condensed components, and thereby enrich more heavily condensed BPCAs (see Vaezzadeh et al., 2023; Notterpek et al., 2025, and references therein). Conversely, less-condensed aromatic clusters with functional side chains (including those produced by aging) may interact more effectively with mineral phases, enhancing their stability and retention compared to highly condensed clusters with fewer functional groups (Schiedung et al., 2020; Pignatello et al., 2024). The relatively low mellitic acid yields obtained in this study, particularly compared to modern charcoals (Notterpek et al., 2025), do not suggest post-depositional inflation of heavily carboxylated BPCAs. The consistent relative distributions of BPCAs in sequence 1, and to a lesser extent sequence 4, further suggest that the translocated PyC fraction was primarily particulate rather than dissolved (Abiven et al., 2011; Santos et al., 2022; Vaezzadeh et al., 2023). Particle-size effects may contribute to the greater proportion of weakly condensed BPCAs with distance from the burned layer in sequences 2 and 3, as smaller PyC molecules are more readily transported (Spokas et al., 2014; Hobley, 2019), though additional research is required to clarify the influence of particle size on diagenetic alterations to aromatic condensation, particularly in aged samples (Abiven et al., 2011; Notterpek et al., 2025).

The total BPCA contents here measured substantially exceed those reported in other archaeological or ancient contexts (e.g., Kappenberg et al., 2019; Chu et al., 2022; Wöstehoff et al., 2022, 2023), reflecting favourable PyC preservation. Beyond the fragmentation and physical transport of PyC through various processes (e.g., thermal alteration, erosion, infiltration), diagenetic alterations to the polycondensed aromatic structures from which BPCAs are oxidised appear minimal, particularly for samples within the burned layer. The HTT values here presented may reflect the maximum temperature attained during pyrolysis, given the manner in which BPCA data are reported and the HTT prediction models were constructed (Notterpek et al., 2025). However, they may also represent the average temperature across the entire pyrolysis process, or alternatively, the temperature maintained for the longest duration during pyrolysis. While further experimental work is required to resolve this uncertainty, the absence of molecular evidence for the selective enrichment of heavily condensed PyC indicates that our values do not overestimate HTT. Further, any systematic model biases affecting HTT prediction accuracy should affect the assemblage uniformly. As such, variability in predicted HTT values — grounded in direct measures of PyC aromaticity and aromatic condensation — is interpreted to reflect genuine differences in the combustion conditions that governed PyC formation during the burn event.

5.1.2. Organic matter preservation

553

554

555

556

557

558

559

560

561

562

563

564

565

566

567

568

569

570

571

572

573

574

575

576

577

Reconstructing past environments or processes through lipid biomarker evidence requires careful interpretation of post-depositional alterations affecting data reliability. In addition to environmental ageing, thermal degradation constitutes an important diagenetic pathway in fire-affected deposits. Lipid preservation was evaluated in this study through proxies indicative of OM maturity, complemented by the identification of degradation markers. While the precise taphonomic process responsible for the observed degradation cannot always be identified given the multitude of potential pathways, several patterns emerge from the available evidence. The results broadly indicate the presence of both thermal and environmental degradation, selective taphonomic pathways

affecting certain compound classes over others, and stratigraphic variation in molecular distributions reflecting a combination of degradation and potential palaeoenvironmental shifts.

578

579

580

581

582

583

584

585

586

587

588

589

590

591

592

593

594

595

596

597

598

599

600

601

602

603

Numerous experimental studies have demonstrated that heat-induced cracking of the carbon bonds forming aliphatic hydrocarbon chains reduces chain lengths, thereby lowering ACL and increasing short- to long-chain ratios (e.g., R_{s/l}, FA_{s/l}) (Almendros et al., 1988; González-Pérez et al., 2008; Wiesenberg et al., 2009; Knicker et al., 2013; Sarangi et al., 2022). Alterations to chain lengths inevitably shift relative proportions of odd and even homologues, measured by the OEP, EOP, and CPI. These values are high in fresh vegetal matter (Eglinton and Hamilton, 1967), and typically decrease with thermal alteration (e.g., CPI_{long}, Wiesenberg et al., 2009). While inter-sequence variation was observed in the present study, shorter-chain homologues were generally more prevalent in deposits beneath the burned layer (Figs S3-S6), reflected quantitatively in the aforementioned proxies. This was most evident for n-alkanes in the transition to/from the burned layer (e.g., OEP, Fig. 7), suggesting that thermal alteration was a significant driver for alkane degradation. Attributing a uniquely thermal origin to this degradation is nevertheless complicated by potential precursor feedstock/tissue effects (e.g., leaves versus wood, Jambrina-Enríquez et al., 2018), combustion conditions (e.g., oxygen availability, Wiesenberg et al., 2009; Knicker et al., 2013), and characteristics of the depositional environment (Thomas et al., 2021). Other aliphatic lipids yielded variable signals (e.g., increased FA_{s/I} with increased EOP) indicating compound-specific diagenetic processes. Still, pyrogenic markers such as APAAs (Bondetti et al., 2021) and likely methyl dehydroabietate (Davara et al., 2023) attest to thermally altered OM. Overall, biomarker evidence suggests that heat modified the molecular fingerprints of available biomass, but the extent of these alterations was not uniform across compound classes or zones of the fire-affected area.

Once deposited, the molecular signal of fresh or charred OM can be rapidly altered with integration into the mineral matrix, and variability is once more observed according to molecule type, precursor OM, pyrolysis conditions (if relevant), and depositional characteristics. Generally, open-system studies demonstrate results resembling those produced by thermal degradation, such as

decreasing n-alkane OEP or n-alkanoic acid EOP with increasing soil residence time (e.g., Hilscher et al., 2009; Knicker et al., 2013; Thomas et al., 2021). The molecular patterns here documented are therefore consistent with both environmental ageing and thermal alteration, making it difficult (and occasionally impossible) to disentangle the two (e.g., Eckmeier and Wiesenberg, 2009; Knicker et al., 2013). Selective preservation processes are also evident, as while n-alkanes exhibit more extensive degradation in the lower deposits (e.g., via OEP and CPI values of ~1), n-alkanol CPI and fatty acid EOP and CPI increase with depth. Intriguingly, FA_{S/I} values also rise in the lowermost deposits, especially within sequence 2 (see also $C_{16:0}/C_{18:0}$, and $C18_{unsat./sat.}$, Fig. 9). While the mechanism(s) behind these patterns remain unclear, these data highlight complex taphonomic pathways differentially affecting each molecule type. Importantly for palaeoenvironmental reconstructions, the enhanced preservation of n-alkanols and fatty acids compared to n-alkanes supports their use as more robust palaeoenvironmental tracers.

Furthermore, we did not detect lipid input from modern roots (Wiesenberg et al., 2010), algae and photosynthetic bacteria (Brocks and Summons, 2003), or microbes (Dudd et al., 1998; Quénéa et al., 2006; Barré et al., 2018). However, the predominance of n-alkanol C_{18} in the control sample (~48%) mirrors observations for the sand fraction of forest and cultivated soils (Quénéa et al., 2006), and may derive from suberin (Nierop et al., 2003), lower plants, or microbial spore lipids (Naafs et al., 2004). This control, located well below the burned layer, provides clear evidence of extensive environmental degradation without pyrogenic interference. Additional evidence for environmentally degraded, plant-derived OM was observed in specific markers, including: dehydroabietic acid from pine resin (Aveling and Heron, 1998); long chain diacids (C_{20} – C_{32} , Fig. S6) and ω -hydroxy acids (C_{20} – C_{24} , Table S1, sheet 7) from suberin (Otto and Simpson, 2006; Lin and Simpson, 2016); and mid-chain ω -hydroxy acids (C_{12} , C_{14}), potentially from cutin (Spielvogel et al., 2014).

Assembled, the diagenetic evidence suggests that the post-depositional translocation of thermally degraded OM down the soil profile provides a more plausible explanation for increased degradation than *in situ* heating during the combustion event. While thermal alteration up to 10 cm

below the soil surface has been reported in both wildfires and experimental studies, the recorded temperatures are generally low (e.g., 95 °C for surface fires, Campbell et al., 1995; Busse et al., 2005; ~200 °C in controlled experiments, Aldeias et al., 2016) and/or insufficiently sustained to account for the observed lipid transformations (see also Jambrina-Enríquez et al., 2018). Instead, vertical translocation of thermally altered OM (principally downward) appears more consistent with the data. Although the hydrophobicity of lipids renders leaching improbable, transport of particle-bound OM via percolating groundwater remains plausible. Lipids may also have been adsorbed by microcharcoal particles and particulate PyC, whose translocation is evidenced by BPCA yields and distributions (section 5.1.1). Such redistribution may have partially masked the endogenous OM signature in the pre-fire deposits, complicating the interpretation of aliphatic lipid distributions, yet not all compound classes were affected equally. Fatty acids and *n*-alkanols exhibit enhanced preservation compared to *n*-alkanes, potentially reflecting preferential stabilisation within organomineral complexes (e.g., Lin and Simpson, 2016; Chang et al., 2020). These findings thus indicate that while *n*-alkane signals require cautious interpretation, fatty acids and alkanols constitute more robust tracers for palaeovegetal and palaeoclimatic reconstructions in these deposits.

5.2. Palaeoenvironmental reconstructions from lipid biomarker evidence

Palaeoenvironmental reconstructions must account for the diagenetic processes outlined in section 5.1. By integrating multiple biomarkers and prioritising those shown to be more resistant to post-depositional alterations, we can extract the most reliable evidence for past vegetation and environmental conditions. The lipid biomarkers here identified provide robust evidence for significant OM input from higher terrestrial plants, including epicuticular waxes. This is supported by aliphatic lipid data indicative of degraded vegetal matter (section 5.1.2), as well as the presence of phytosterols common to higher plants (e.g., stigmasterol, stigmastanol, β -sitosterol) (Volkman, 2005). Together, these data indicate a vegetation shift from a conifer-dominant forest with scattered deciduous species (e.g., boreal forest) to a more mosaic post-burn landscape with greater contributions from deciduous trees, grasses, and herbaceous taxa (e.g., temperate broadleaf or mixed forest).

5.2.1. Palaeoenvironmental conditions prior to and at the moment of the combustion event

656

657

658

659

660

661

662

663

664

665

666

667

668

669

670

671

672

673

674

675

676

677

678

679

680

681

Anthracological evidence from survey 95 demonstrates that the biomass affected by the burn event, and thus established in the landscape at the time of the fire, was composed mainly of pine (*Pinus* cf. *sylvestris/nigra*) with sparse birch trees. This assemblage suggests a relatively open environment with cool climatic conditions.

Among the biomolecular evidence, terpenoids provide the most taxonomically informative data and corroborate anthracological identifications. The detected abietane-class compounds (e.g., abietic acid, dehydroabietic acid, methyl dehydroabietate) are tricyclic diterpenoids, which are common in gymnosperms and particularly prevalent in pine resins (Otto and Simoneit, 2001; Hjulström et al., 2006; Diefendorf et al., 2012; Davara et al., 2023). Dehydroabietic acid is frequently the most abundant resin acid in soils and sediments beneath pine forests (Almendros et al., 1988; Nierop et al., 2006), and its concentration has been shown to increase with heating (Diefendorf et al., 2015b; Davara et al., 2023). Methyl dehydroabietate may further indicate the "hard heating" of pine wood, rather than resin alone (Davara et al., 2023). Pentacyclic triterpenoids are typically found in angiosperms, and while often not family-specific, lupane and lupane-type markers are especially abundant in birch bark (Simoneit, 1986; Aveling and Heron, 1998). In the study of archaeological adhesives, the co-occurrence of these markers (e.g., betulin, lupeol, betulinic acid) is diagnostic of birch bark tar (Lucquin et al., 2007; Koch et al., 2024). Several of the identified markers (e.g., betulone, lupa-2,20(29)-dien-28-ol) are experimentally associated with the "soft heating" of birch bark, though they may also derive from natural decay (Aveling and Heron, 1998), and no markers associated with "strong heating" were detected (Rageot et al., 2019).

Although aliphatic lipid data is often less taxonomically specific than terpenoids or anthracology, n-alkane and n-alkanoic acid results similarly indicate a forested pre-fire landscape with minimal input from grasses and herbaceous materials. For example, n-alkane distributions (Table S1, sheet 4 and Fig. S3) and ACL values (Fig. 7) below the burned layer trend toward the dominant homologues documented in trees (C_{27} and C_{29}) rather than those observed in grasses (C_{31} and C_{33})

(Poynter et al., 1989; van Bergen et al., 1997). *n*-Alkane ACL_{long} values in and below the burned layer (including the control and M13 2) align with those reported by Schäfer et al. (2016) in coniferous litter (~28.6–29.8) and topsoil horizons (~29.8–30.3), as well as deciduous forest horizons (particularly topsoil, ~29.0–29.7), from sites in central and southeast Europe. *n*-Alkane ratios similarly correspond to reference values for coniferous and deciduous forest horizons, particularly deciduous forest topsoils at 0–3 cm depth (~0.17–0.68) (Schäfer et al., 2016).

The variability of conifer values reported in the literature (e.g., Schäfer et al., 2016; Nezhad et al., 2024) reflects the difficulty of detecting this vegetation type via *n*-alkanes, given their lower abundance in conifers compared to angiosperms (Diefendorf et al., 2011, 2015a). Accordingly, other aliphatic compounds such as *n*-alkanoic acids provide more reliable evidence for conifer contributions to OM. The pre-fire presence of conifers is supported by fatty acid CDI results, which cluster toward the maximum value observed in coniferous forest horizons in the study of Schäfer et al. (2016): 0.91 (Fig. 10). For comparison, maximum values of 0.62 were documented in deciduous forests (CDI-D) and 0.37 in grasslands (CDI-G); higher values are systematically associated with stronger correlations to these vegetal sources and a greater ability to distinguish between them, even across different soil horizons (Schäfer et al., 2016). These results therefore suggest that pre-burn OM contributions were predominantly tree-derived, with greater input from conifers than deciduous species, and very minimal contributions from grasses.

n-Alkanol distributions are similarly consistent with higher plants (Kolattukudy, 1980), particularly suberized tissues (C_{16} – C_{24}) in samples below the burned layer (Kolattukudy, 2001). While primarily reflective of vegetal inputs to SOM, n-alkanols have also been proposed as palaeoclimatic indicators given potential correlations between n-alkanol proxies (ACL, CPI, alkanol index) and magnetic susceptibility. Higher magnetic susceptibility is positively correlated with warmer interstadial conditions and increased precipitation (Maher, 1998; Herries, 2006; Balsam et al., 2011), and has been observed to correlate with lower CPI, higher ACL, and higher alkanol index values (Zhang et al., 2006). Further, the ratio C_{24}/C_{26} may be inversely correlated with precipitation (Zheng et al., 2009). In the

present study, n-alkanol results below the burned layer are consistent with cold and arid climatic conditions, as evidenced by: (i) low ACL (< 28, $\Sigma C_{24-32 \text{ even}}$) and alkanol index (< 0.35) values, which are consistent with those observed for glacial periods (MIS 6 and 4) in the loess sequence studied by Zhang et al. (2006); (ii) high CPI values (supplementary information); and (iii) elevated C_{24}/C_{26} values.

However, these palaeoclimatic interpretations must remain tentative given the limited number of studies exploring *n*-alkanol–climate relationships, many of which derive from environmental contexts far removed from the present study area (e.g., Rommerskirchen et al., 2003; Zhang et al., 2006; Zheng et al., 2009). Further studies are needed to corroborate these observations, particularly in fire-affected terrestrial records (for palaeovegetal studies in lacustrine and peat deposits, see Zheng et al., 2007; Zhou et al., 2010; Zhang et al., 2021, and references therein). Acknowledging the need for local calibration and the potential effects of diagenetic alteration on the observed signal (section 5.1.2), the evidence for cool and dry climatic conditions is nevertheless consistent with anthracological impressions of a *Pinus*-dominated boreal forest.

A final evidentiary lens, indicative of palaeovegetation at the moment of the combustion event, is that of BPCA-derived precursor feedstock predictions. While predictions extend beyond the macroscopic burned layer(s), this is likely due to the translocation of microcharcoal particles and molecular PyC (section 5.1.1), with all BPCAs derived from pyrogenic OM. Non-pyrogenic interference — for instance from petrogenic sources, humic acids, or plant biopolymers with non-condensed aromatic structures (e.g., lignin) (review in Vaezzadeh et al., 2023; Notterpek et al., 2025) — is negligible as: (i) petrogenic source material and humic acids were absent from the studied layers; (iii) sample OC contents were limited (Kappenberg et al., 2016; Di Rauso Simeone et al., 2024), and (iv) potential contributions, such as B3CA from lignin (Di Rauso Simeone et al., 2024), are mitigated by the full BPCA distribution being required for the random forest model (Notterpek et al., 2025). However, the accuracy level of this algorithm is lower than that of HTT (qualitative), at approximately 60% versus 80% (Notterpek et al., 2025). The results (Fig. 12 and Table S1, sheet 9) also demonstrate a possible conflation with HTT, as low-temperature samples tend to yield higher grass probabilities. These

limitations underscore the need for caution whilst model accuracy and taxonomic coverage are improved. Nonetheless, this method holds potential in its ability to estimate precursor feedstock contributions to microcharcoal and molecular PyC that are not amenable to anthracological study.

5.2.2. Post-fire palaeoenvironmental conditions: temperate broadleaf or mixed forest

While no anthracological data is available for the post-fire deposits, lipid biomarkers indicate a shift in OM contributions in samples overlying the burned layer marked by a contraction of coniferous vegetation, alongside the expansion of deciduous trees and grasses/herbaceous taxa.

Post-fire grass expansion is suggested in *n*-alkanes by increased C₃₁ and C₃₃ contributions above the burned layer (Fig. S3) (Poynter et al., 1989; van Bergen et al., 1997). Both ACL_{long} and *n*-alkane ratios correspond to grassland topsoil values (ACL_{long}: ~30.1–30.4, *n*-alkane ratio: 0.73–0.83) in these overlying samples, with the exception of M13 5 (Fig. 7), which overlaps with the high end of coniferous and deciduous forest values reported by Schäfer et al. (2016). These patterns may partly reflect taphonomic effects and highlight the difficulty of interpreting degraded Pleistocene samples (indicated by low OEP values) using modern references and calibration curves, as demonstrated by the erratic results produced by end-member modelling of grass contributions (Zech et al., 2013; Schäfer et al., 2016) (Table S1, sheet 4). Fatty acids, being better preserved than *n*-alkanes in survey 95 (section 5.1.2) and more sensitive to vegetation change involving conifers, provide stronger evidence for this shift. Compared to the pre-fire deposits, CDI results above the burned layer are tightly clustered (Fig. 10) and indicate reduced conifer input (lower CDI-C), additional deciduous contributions (higher CDI-D), and increased grass/herbaceous input (higher CDI-G).

The increase in n-alkanol chain lengths above the burned layer reinforces these trends, with the predominance of C_{26} (Fig. S4) likely reflecting enhanced grass input (van Bergen et al., 1997; Naafs et al., 2004). This increase, expressed in ACL and alkanol index results, may also signal broader palaeoclimatic changes. Specifically, increasing ACL (on the order of ~ 0.74 with the calculation of Zhang et al., 2006; and ~ 1.56 with that of Zheng et al., 2009), decreasing CPI (supporting information), and alkanol index values typical of interstadial periods (> 0.4, Zhang et al., 2006) suggest a shift toward

warmer climatic conditions following the burn event. A concurrent decrease in C_{24}/C_{26} indicates increased moisture or humidity (Zheng et al., 2009). While these signals cannot be interpreted as direct climatic evidence without local calibration and complementary data, they contrast with the pre-fire signal and are consistent with vegetation changes indicated by other aliphatic lipids, involving a retraction of conifers (namely *Pinus*) and expansion of deciduous taxa, grasses and herbaceous plants.

760

761

762

763

764

765

766

767

768

769

770

771

772

773

774

775

776

777

778

779

780

781

782

783

784

Taken as a whole, palaeovegetal and palaeoclimatic data indicate a transition from a cool, Pinus-dominant boreal forest ecosystem to a warmer, more humid environment with temperate broadleaf or mixed forest characteristics. While chronometric control of the studied deposits are limited, with a terminus ante quem of 90.4 ± 6 ka, these shifts suggest a transition from stadial or cool interstadial periods to warmer interstadial conditions. If the deposits can be more narrowly constrained to MIS 5c, associated with the Brörup interstadial (Müller et al., 2003), the observed shifts may correspond to specific warming events. Based on the available data, we tentatively propose the transition from St. Germain Ia, which includes a short cold phase known as the Montaigu event (Woillard, 1978) marked by Pinus expansion (Müller et al., 2003; Helmens, 2014), to St. Germain Ic (Wohlfarth, 2013). Given the large number of fluctuations observed in Greenland ice-core records between ~90 and 110 ka (Rasmussen et al., 2014), and the limited chronological resolution of deposits, we do not attempt to link the studied sequence to individual stadial-interstadial events. Instead, this hypothesis rests on broader palaeovegetal and palynological data observed in nearby terrestrial records such as La Grande Pile (Woillard, 1978) and Les Echets (Beaulieu and Reille, 1984). Further refinement will require both higher-resolution chronometric data and palaeoclimatic evidence derived from additional methods.

5.3. Reconstructing the fire event in survey 95

With the data at hand, the natural or anthropogenic origins of these combustion traces can be evaluated through three primary lenses: (i) macroscopic and anthracological evidence, (ii) molecular evidence, and (iii) char production parameters, specifically HTT.

5.3.1. Macroscopic and anthracological evidence

From a geological and archaeological point of view, the quantity of combustion residues and their characteristics support the hypothesis of a wildfire. For instance, no macroscopic evidence for a concentrated zone of combustion residues surrounded by more dispersed areas (as could be envisioned for certain anthropogenic fires) were identified. This does not, however, negate the possibility of *in situ* combustion features masked by a subsequent natural fire, or of large-scale anthropogenic fires for other intended purposes (e.g., smoke signalling, site abandonment). Because wildfires (including ground, surface and crown fires) generate diverse macroscopic charcoal remains, closer examination of the anatomical features of the charcoal assemblage may provide a more reliable basis for distinguishing these fire regimes.

Ground fires consume heterogeneous, small-calibre fuels (e.g., roots) and other SOM below the ground surface under limited oxygen supply, resulting in a high degree of incomplete carbonisation (Rein et al., 2008; Watts and Kobziar, 2013). Surface fires involve the combustion of dead litter accumulations and low-lying surface biomass (i.e., brush, twigs) under low to medium oxygenated conditions, and generally produce large quantities of charcoal (Albini, 1993; Stocks and Kauffman, 1997; Scott, 2010). Crown fires describe the combustion of canopy biomass, often initiated by surface fires or lightning strikes, and are common in conifer forests (Van Wagner, 1977). They typically burn only twigs and needles, generating significant amounts of microcharcoal in smoke but limited macrocharcoal remains (e.g., partially charred tree trunks) (Komarek et al., 1973; Stocks and Kauffman, 1997). Ground fires may accompany crown fires, particularly in areas where underlying soils contain substantial humus or peat deposits, and can burn for prolonged periods (Komarek et al., 1973; Pyne et al., 1996; Scott, 2010).

For all wildfire types, the degree of fuel heterogeneity is contingent upon the diversity of available biomass. As the assemblage of survey 95 is strongly *Pinus* dominated, wood taxonomy provides limited insight into fire type, highlighting the importance of anatomical features. However, direct comparisons between contemporary fire observations and ancient charred remains must be

treated with caution. Interpretations of anatomical signatures should carefully consider the range of post-depositional processes that may have altered the original charcoal assemblage, which was formed in a biased and incomplete manner. Nevertheless, the anthracological data from Ormesson casts doubt on the likelihood of a crown fire given the abundant macrocharcoal remains, which feature a high proportion of branch wood (48%) and small proportion of green wood (7%). Yet based on this evidence, we cannot negate the possibility that the charcoal assemblage was formed by the combustion of surface vegetation during a crown wildfire. The high proportion of branch wood and low proportion of dead wood (13%) further indicate a distinctive formation process, particularly as dead wood generally constitutes the majority of fuel utilised by Palaeolithic societies (Théry-Parisot, 2001).

The primary anatomical feature observed in the charcoal assemblage was vitrification, the origins of which remain debated. Although vitrification is closely associated with combustion (i.e., it cannot occur without carbonisation), other factors such as the characteristics of the wood (e.g., physiological state) and/or particular combustion conditions appear necessary to produce cellular fusion. Several hypotheses have been proposed for vitrification, including high pyrolysis temperatures (McParland et al., 2010), high wood moisture content (Prior and Alvin, 1986; Henry, 2011), oxygenstarved combustion (Fabre, 1996), or other specific combustion conditions (Vidal-Matutano et al., 2019, 2020; Courty et al., 2020). However, these hypotheses currently lack strong experimental support (Théry-Parisot, 2001; McParland et al., 2010). The high proportion of vitrification here observed (67%) is notable compared to other archaeological contexts, where it is typically observed in less than 5% of the charcoal assemblage. While the high frequency of vitrification and low proportion of dead wood attest to the unique nature of the combustion event, these features are insufficient to determine whether the fire was natural or anthropogenic, or to identify the wildfire type best correlated with the macroscopic charcoal remains.

5.3.2. Molecular evidence

The molecular discrimination of natural and human-controlled fires has been principally pursued through the analysis of PAH and BPCA distributions (e.g., Wolf et al., 2013; Brittingham et al., 2019; Stancampiano et al., 2023). Pyrogenic lipid biomarkers formed within precise temperature ranges are also informative, as they may aid reconstructions of HTT (e.g., Jambrina-Enríquez et al., 2019). For instance, as APAAs are formed by the heating of unsaturated fatty acids at temperatures above 270 °C for 1 h or 200 °C for 5 h (Hansel et al., 2004; Admiraal et al., 2019; Bondetti et al., 2021), the trace presence of these compounds provides molecular evidence for the thermal alteration of unsaturated fatty acids above at least 200 °C. However, these pyrogenic markers attest only to pyrolysis, not to the specific origin of the combustion process.

In the case of BPCA analysis, recent work (Notterpek et al., 2025) has shown that the ratio of B5CA/B6CA is indeed correlated with HTT, but is not reliable for the reconstruction of past fire regimes (Wolf et al., 2013). Other BPCA outputs are more significantly correlated with HTT, and robust HTT reconstruction requires integrating multiple quantitative outputs (Notterpek et al., 2025). Furthermore, we must reckon with the heterogeneity of combustion events and develop methods to account for this heterogeneity in ancient samples, both in relation to the initial combustion event and subsequent post-depositional alterations. Archaeological interpretations of PAH distributions (light versus heavy) to reconstruct hominin fire activity (e.g., Brittingham et al., 2019) are subject to the same caveats, as these distributions must be interpreted in light of taphonomy as well as understandings of wildfire particle emissions that continue to be refined (e.g., Denis et al., 2012; Argiriadis et al., 2018).

A greater abundance of heavy PAHs or heavily carboxylated BPCAs reflects PyC characteristics, such as increased aromatic condensation (due to high HTT, oxygen-starved combustion, etc.), rather than the origin of these pyrogenic markers. No unambiguous "anthropogenic" fire markers have yet been identified, and even if seemingly anthropic markers were detected, their presence could be explained by non-human factors — for instance, heated animal fats from carcasses, or resin acids from conifer trees naturally present in the fire-affected area. Molecular evidence for pyrolysis at Ormesson

is therefore inconclusive, though such data may acquire greater discriminatory power when supported by additional studies of molecular heterogeneity in natural and human-controlled fires, and the effects of environmental diagenesis on these molecular signals.

5.3.3. Char production parameters (HTT)

The final evidentiary lens with the potential to distinguish natural and anthropogenic fires is that of char production parameters, which broadly encompass factors such as precursor feedstock type, oxygen availability, combustion duration, and HTT. This prospect is complicated, however, by the substantial variability of these parameters within a single combustion event (whether natural or anthropogenic) and the difficulty of disentangling these variables in molecular or other archaeometric analyses. Among these factors, HTT currently appears most promising given the extensive experimental measurements available for wildfires and human-controlled combustions, which constitute a robust reference corpus against which HTT estimates from unknown samples can be compared.

To contextualise HTT values, it is constructive to consider the range of temperatures reported for different wildfire types. Ground fires have relatively low combustion temperatures of ≤ 300 °C (Rundel, 1981, 1983), though higher temperatures of up to 600 °C (averaging 400 °C) have been documented (Usup et al., 2004; Rein et al., 2008). Surface wildfires reach temperatures of approximately ≤ 350 °C in the litter layer (median: 283 ± 134 °C per Wolf et al. 2013), including grasses and other herbaceous materials (Albini, 1993; Stocks and Kauffman, 1997), but may reach higher temperatures (~600 °C) elsewhere that persist for several hours (Pyne et al., 1996). Shrubland surface fires are associated with higher combustion temperatures of approximately 450 °C (median: 503 ± 211 °C per Wolf et al. 2013). Crown fire combustion temperatures vary widely in the literature, but these fires generally burn hotter (approximately 800–900 °C) than ground or surface fires, with reports of air temperatures peaking as high as 1330 °C (Butler et al., 2004; Doerr et al., 2018). Acknowledging the diversity of actualistic wildfire combustion temperatures due to environmental factors (e.g.,

atmospheric humidity), we can generally predict temperatures of < 600 °C for ground and surface fires and > 800 °C for crown fires.

Experimental archaeological research has documented a wide range of temperatures associated with different hearths, with average and maximum combustion temperatures (as well as flame duration, luminosity, radiative heat output, etc.) conditioned by a host of factors not limited to: hearth shape and size, fuel type and condition, environmental constraints, and maintenance behaviours (Sievers and Wadley, 2008; Braadbaart et al., 2012; March et al., 2014; Aldeias, 2017). Nevertheless, average combustion temperatures of 250–550 °C and maximum temperatures of 460–800 °C are documented in conventional open-air hearths (Théry-Parisot et al., 2025). Per the review of Wolf et al. (2013), domestic fires were associated with higher median temperatures of 797 ± 165 °C.

Consequently, expected temperature ranges for anthropogenic hearths and ground/surface wildfires overlap between 250 and 550 °C. The BPCA-derived HTT estimates here presented fall precisely within this range, at approximately 300–400 °C for charcoal samples and 400–550 °C for soil samples. These values are therefore consistent with surface wildfire temperatures, including those coinciding with crown fires, as well as human-controlled, open-air hearths. While reconstructed temperature data has been utilised to identify low-temperature surface fires, with sporadic high measurements attributed to possible canopy combustion (Marynowski et al., 2011), the ability of HTT to discriminate between anthropogenic fires and most wildfire types thus appears limited. This limitation is compounded by diagenetic alterations to the material from which HTT estimations are derived, which impact the reliability of HTT predictions, as shown for elemental analysis (Mouraux et al., 2022) and the Raman–HRTEM method (Deldicque et al., 2023; Delarue et al., 2024) in charcoal. As discussed in section 5.1.1, uncertainty also persists regarding the specific temperature measured by these proxies. Further research is required to resolve these uncertainties and, as for molecular distributions, to develop approaches that account for heterogeneity in combustion processes and their resultant residues.

6. Conclusion

Our multiproxy analyses have demonstrated several key points for the interpretation of these fire traces, notably that:

- The charcoal assemblage is dominated by *Pinus* cf. *sylvestris/nigra*, with some *Betula* sp. and gymnosperm taxa. The charcoals exhibit a significant degree of vitrification (67%) with high amounts of branch wood (48%), and smaller amounts of dead wood (13%) and evidence for green wood combustion (7%).
- Higher terrestrial plants are a significant contributor to SOM, with biomolecular evidence for the presence of conifer trees (e.g., Pinaceae, via diterpenoid resin acids) and angiosperm species (e.g., birch, via lupane-family pentacyclic triterpenoids). Following the burn event, the local environment likely saw a reduction in conifer species and an increase in deciduous trees and grassy/herbaceous vegetation.
- The combustion produced significant quantities of PyC, with BPCA contents of up to 362 g BPCA-C/kg OC in soil samples and 443 g BPCA-C/kg OC in charcoal samples, and aromatic condensation values of up to 34%. HTT predictions derived from BPCA results indicate combustion temperatures of approximately 300–400 °C in charcoal samples and 400–550 °C in soil samples from the burned layer.

Mobilising this data to determine the nature of the combustion event requires careful consideration of the identification criteria for past fire traces, yet this study has demonstrated the substantial equifinality of archaeometric and geochemical data from natural and anthropogenic fires. This highlights a broader methodological issue, in that clear diagnostics for differentiating these fire types do not currently exist. Past fire traces are often interpreted on the basis of geological and archaeological observations, without geochemical and molecular support, despite the abundance of molecular data held within soil and sedimentary matrices. This can be justified in cases such as clearly structured hearths within the archaeological deposits of a cave site. However, cases such as Ormesson featuring extensive combustion residues in an open-air context, or the Caune de l'Arago with scattered fire traces in a cave site (Deldicque et al., 2021), encourage rigorous engagement with the null

hypothesis: that the combustion residues are non-anthropogenic in origin. In light of all available evidence, we accept this null hypothesis and thus do not attribute an anthropic origin to these combustion residues.

This wildfire, in a landscape dominated by *Pinus* spp., was likely intense given the sheer quantity of combustion residues and PyC produced. However, BPCA-derived temperature estimates fall in the expected ranges for both anthropic and natural fire types. Further research is needed to better characterise alterations to the BPCA signal through environmental degradation and to determine how post-depositional processes, such as the selective preservation of weakly condensed PyC (via organomineral interactions), may impact HTT estimates. Experimental research into the factors producing charcoal vitrification will also help clarify the exceptional combustion conditions of this previously unknown wildfire in the Paris Basin region during the Early Weichselian glacial period (MIS 5). More broadly, archaeological and environmental scientists must establish rigorous, systematic guidelines for interpreting past fire traces that address the challenges of equifinality. In doing so, we will be able to harness the full potential of macroscopic, microscopic, and molecular data in ancient and archaeological combustion residues. This is particularly important for analysing the oftenephemeral fire traces of the Pleistocene, so critical to understanding the evolution of pyrotechnology among Pleistocene and Palaeolithic hominins.

962

963

964

965

966

969

970

971

974

975

976

977

978

984

985

986 987

988

991

992

- Abiven, S., Hengartner, P., Schneider, M.P.W., Singh, N., Schmidt, M.W.I., 2011. Pyrogenic carbon
 soluble fraction is larger and more aromatic in aged charcoal than in fresh charcoal. Soil Biol.
 Biochem. 43, 1615–1617.
- Abney, R.B., Berhe, A.A., 2018. Pyrogenic carbon erosion: Implications for stock and persistence of pyrogenic carbon in soil. Front. Earth Sci. 6, 335325.
 - Admiraal, M., Lucquin, A., von Tersch, M., Jordan, P.D., Craig, O.E., 2019. Investigating the function of prehistoric stone bowls and griddle stones in the Aleutian Islands by lipid residue analysis. Quat. Res. 91, 1003–1015.
 - Albini, F.A., 1993. Dynamics and modeling of vegetation fires: observations, in: Crutzen, P.J., Goldammer, J.G. (Eds.), Fire in the Environment: The Ecological, Atmospheric and Climatic Importance of Vegetation Fires. Wiley, Chicester, pp. 39–52.
- Aldeias, V., 2017. Experimental approaches to archaeological fire features and their behavioral relevance. Curr. Anthropol. 58, S191–S205.
 - Aldeias, V., Dibble, H.L., Sandgathe, D., Goldberg, P., McPherron, S.J.P., 2016. How heat alters underlying deposits and implications for archaeological fire features: A controlled experiment. J. Archaeol. Sci. 67, 64–79.
- 972 Almendros, G., Martín, F., González-Vila, F.J., 1988. Effects of fire on humic and lipid fractions in a 973 Dystric Xerochrept in Spain. Geoderma 42, 115–127.
 - Alperson-Afil, N., 2012. Archaeology of fire: Methodological aspects of reconstructing fire history of prehistoric archaeological sites. Earth Sci. Rev. 113, 111–119.
 - Argiriadis, E., Battistel, D., McWethy, D.B., Vecchiato, M., Kirchgeorg, T., Kehrwald, N.M., Whitlock, C., Wilmshurst, J.M., Barbante, C., 2018. Lake sediment fecal and biomass burning biomarkers provide direct evidence for prehistoric human-lit fires in New Zealand. Sci. Rep. 8, 12113.
- 979 Aveling, E.M., Heron, C., 1998. Identification of birch bark tar at the Mesolithic site of Star Carr. Anc. 980 Biomol. 2, 69–80.
- 981 Balsam, W.L., Ellwood, B.B., Ji, J., Williams, E.R., Long, X., El Hassani, A., 2011. Magnetic susceptibility 982 as a proxy for rainfall: Worldwide data from tropical and temperate climate. Quat. Sci. Rev. 30, 983 2732–2744.
 - Barbetti, M., 1986. Traces of fire in the archaeological record, before one million years ago? J. Hum. Evol. 15, 771–781.
 - Barré, P., Quénéa, K., Vidal, A., Cécillon, L., Christensen, B.T., Kätterer, T., Macdonald, A., Petit, L., Plante, A.F., van Oort, F., Chenu, C., 2018. Microbial and plant-derived compounds both contribute to persistent soil organic carbon in temperate soils. Biogeochemistry 140, 81–92.
- 989 Beaulieu, J.-L. de, Reille, M., 1984. A long Upper Pleistocene pollen record from Les Echets, near Lyon, 990 France. Boreas 13, 111–132.
 - Belcher, C.M., Stacey L. New, Santín, C., Doerr, S.H., Dewhirst, R.A., Grosvenor, M.J., Hudspith, V.A., 2018. What can charcoal reflectance tell us about energy release in wildfires and the properties of pyrogenic carbon? Front. Earth Sci. 6, 389593.
- 994 Bellè, S.-L., Berhe, A.A., Hagedorn, F., Santin, C., Schiedung, M., van Meerveld, I., Abiven, S., 2021. Key 995 drivers of pyrogenic carbon redistribution during a simulated rainfall event. Biogeosciences 18, 996 1105–1126.
- 997 Berna, F., Goldberg, P., Horwitz, L.K., Brink, J., Holt, S., Bamford, M., Chazan, M., 2012. 998 Microstratigraphic evidence of in situ fire in the Acheulean strata of Wonderwerk Cave, 999 Northern Cape province, South Africa. Proc. Natl. Acad. Sci. U.S.A. 109, E1215-20.
- Bird, M.I., Brand, M., Comley, R., Fu, X., Hadeen, X., Jacobs, Z., Rowe, C., Wurster, C.M., Zwart, C., Bradshaw, C.J.A., 2024. Late Pleistocene emergence of an anthropogenic fire regime in Australia's tropical savannahs. Nat. Geosci. 17, 233–240.
- Bodu, P., Dumarçay, G., Naton, H.-G., 2014a. Un nouveau gisement solutréen en Île-de-France, le site des Bossats à Ormesson (Seine-et-Marne). Bull. Soc. préhist. fr. 111, 225–254.

- Bodu, P., Naton, H.-G., 2024. On a perdu l'Aurignacien ! Questionnement sur les présences/absences et autres hiatus sur le site préhistorique des Bossats à Ormesson (Seine-et-Marne, France), in:
 Hiatus, lacunes et absences : identifier et interpréter les vides archéologiques. Actes du 29e
 Congrès préhistorique de France, 31 mai-4 juin 2021, Toulouse. Société préhistorique française, Paris, pp. 5–30.
- Bodu, P., Salomon, H., Lacarrière, J., Baillet, M., Ballinger, M., Naton, H.-G., Théry-Parisot, I., 2017. Un gisement châtelperronien de plein air dans le Bassin parisien : les Bossats à Ormesson (Seine-et-Marne). Gall. préhistoire 57, 3–64.
- Bodu, P., Salomon, H., Leroyer, M., Naton, H.-G., Lacarriere, J., Dessoles, M., 2014b. An open-air site from the recent Middle Palaeolithic in the Paris Basin (France): Les Bossats at Ormesson (Seine-et-Marne). Quat. Int. 331, 39–59.
- 1016 Bondetti, M., Scott, E., Courel, B., Lucquin, A., Shoda, S., Lundy, J., Labra-Odde, C., Drieu, L., Craig, O.E., 1017 2021. Investigating the formation and diagnostic value of ω -(o-alkylphenyl)alkanoic acids in ancient pottery. Archaeometry 63, 594–608.

1020

1021

1022

10231024

1025

1026

1027

1028

1029

1030

1031

1032

1033

1034

1035

1038

- Braadbaart, F., Poole, I., Huisman, H.D.J., van Os, B., 2012. Fuel, Fire and Heat: an experimental approach to highlight the potential of studying ash and char remains from archaeological contexts. J. Archaeol. Sci. 39, 836–847.
 - Braadbaart, F., Reidsma, F.H., Roebroeks, W., Chiotti, L., Slon, V., Meyer, M., Théry-Parisot, I., van Hoesel, A., Nierop, K.G.J., Kaal, J., van Os, B., Marquer, L., 2020. Heating histories and taphonomy of ancient fireplaces: A multi-proxy case study from the Upper Palaeolithic sequence of Abri Pataud (Les Eyzies-de-Tayac, France). J. Archaeol. Sci. Rep. 33, 102468.
- Brittingham, A., Hren, M.T., Hartman, G., Wilkinson, K.N., Mallol, C., Gasparyan, B., Adler, D.S., 2019. Geochemical evidence for the control of fire by Middle Palaeolithic hominins. Sci. Rep. 9, 15368.
- Brocks, J.J., Love, G.D., Summons, R.E., Knoll, A.H., Logan, G.A., Bowden, S.A., 2005. Biomarker evidence for green and purple sulphur bacteria in a stratified Palaeoproterozoic sea. Nature 437, 866–870.
- Brocks, J.J., Summons, R.E., 2003. Sedimentary hydrocarbons, biomarkers for early life, in: Holland, H.D., Turekian, K.K. (Eds.), Treatise on Geochemistry. Elsevier, Oxford, pp. 63–115.
 - Brodowski, S., John, B., Flessa, H., Amelung, W., 2006. Aggregate-occluded black carbon in soil: Occluded black carbon in soil. Eur. J. Soil Sci. 57, 539–546.
- Buggle, B., Wiesenberg, G.L., Glaser, B., 2010. Is there a possibility to correct fossil *n*-alkane data for postsedimentary alteration effects? Appl. Geochem. 25, 947–957.
 - Busse, M.D., Hubbert, K.R., Fiddler, G.O., Shestak, C.J., Powers, R.F., 2005. Lethal soil temperatures during burning of masticated forest residues. Int. J. Wildland Fire 14, 267–276.
- Butler, B.W., Cohen, J., Latham, D.J., Schuette, R.D., Sopko, P., Shannon, K.S., Jimenez, D., Bradshaw, L.S., 2004. Measurements of radiant emissive power and temperatures in crown fires. Can. J. For. Res. 34, 1577–1587.
- 1043 Campbell, G., Jungbauer, J., Bristow, K., Hungerford, R., 1995. Soil temperature and water content 1044 beneath a surface fire. Soil Science 159, 363–374.
- 1045 Certini, G., 2005. Effects of fire on properties of forest soils: a review. Oecologia 143, 1–10.
- 1046 Chang, Z., Tian, L., Li, F., Wu, M., Steinberg, C.E.W., Pan, B., Xing, B., 2020. Organo-mineral complexes 1047 protect condensed organic matter as revealed by benzene-polycarboxylic acids. Environ. 1048 Pollut. 260, 113977.
- 1049 Chrzazvez, J., Théry-Parisot, I., Fiorucci, G., Terral, J.-F., Thibaut, B., 2014. Impact of post-depositional 1050 processes on charcoal fragmentation and archaeobotanical implications: experimental 1051 approach combining charcoal analysis and biomechanics. J. Archaeol. Sci. 44, 30–42.
- 1052 Chu, W., McLin, S., Wöstehoff, L., Ciornei, A., Gennai, J., Marreiros, J., Dobos, A., 2022. Aurignacian 1053 dynamics in Southeastern Europe based on spatial analysis, sediment geochemistry, raw 1054 materials, lithic analysis, and use-wear from Românești-Dumbrăvița. Sci. Rep. 12, 14152.
- 1055 Courty, M.-A., Allue, E., Henry, A., 2020. Forming mechanisms of vitrified charcoals in archaeological firing-assemblages. J. Archaeol. Sci. Rep. 30, 102215.

- 1057 Craig, O.E., Saul, H., Lucquin, A., Nishida, Y., Taché, K., Clarke, L., Thompson, A., Altoft, D.T., Uchiyama, 1058 J., Ajimoto, M., Gibbs, K., Isaksson, S., Heron, C.P., Jordan, P., 2013. Earliest evidence for the 1059 use of pottery. Nature 496, 351-354.
- 1060 Czimczik, C.I., Masiello, C.A., 2007. Controls on black carbon storage in soils. Global Biogeochem. Cycles 1061 21, GB3005.
- Davara, J., Jambrina-Enríquez, M., Rodríguez de Vera, C., Herrera-Herrera, A.V., Mallol, C., 2023. 1062 Pyrotechnology and lipid biomarker variability in pine tar production. Archaeol. Anthropol. Sci. 1063 1064
- 1065 Delarue, F., Ghavidel, A., Quénéa, K., Bellot-Gurlet, L., Rocha, E., Coubray, S., Baudin, F., Sebag, D., 1066 Lemoine, M., Aubry, E., Savignac, F., Dufraisse, A., 2024. Short-term modifications in the 1067 chemical structure of wood charcoals: Implications for anthracological investigations. J. 1068 Archaeol. Sci. Rep. 57, 104672.
- 1069 Deldicque, D., Pozzi, J.-P., Perrenoud, C., Falguères, C., Mahieux, G., Lartigot-Campin, A.-S., Rouzaud, J.-N., 2021. Search for early traces of fire in the Caune de l'Arago at Tautavel (Eastern Pyrenees, France), combining magnetic susceptibility measurements, microscopic observations, and Raman analysis. C. R. Geosci. 353, 247-264.

1071

1072

1073

1074

1075

1076

1077

1078

1079

1080

1081 1082

1083

1084

1085

1086 1087

1088

1089

1090

1091

1092

1093

1094

1097

1098

1099

- Deldicque, D., Rouzaud, J.-N., Vandevelde, S., Medina-Alcaide, M.Á., Ferrier, C., Perrenoud, C., Pozzi, J.-P., Cabanis, M., 2023. Effects of oxidative weathering on Raman spectra of charcoal and bone chars: consequences in archaeology and paleothermometry. C. R. Geosci. 355, 1–22.
- Deldicque, D., Rouzaud, J.-N., Velde, B., 2016. A Raman HRTEM study of the carbonization of wood: A new Raman-based paleothermometer dedicated to archaeometry. Carbon 102, 319-329.
- Denis, E.H., Toney, J.L., Tarozo, R., Scott Anderson, R., Roach, L.D., Huang, Y., 2012. Polycyclic aromatic hydrocarbons (PAHs) in lake sediments record historic fire events: Validation using HPLCfluorescence detection. Org. Geochem. 45, 7–17.
- Di Rauso Simeone, G., Maennicke, H., Bromm, T., Glaser, B., 2024. Artificial formation of benzene polycarboxylic acids during sample processing of black carbon analysis: the role of organic carbon amount. Chem. Biol. Technol. Agric. 11, 1-11.
- Dibble, H.L., Abodolahzadeh, A., Aldeias, V., Goldberg, P., McPherron, S.P., Sandgathe, D.M., 2017. How did hominins adapt to ice age Europe without fire? Curr. Anthropol. 58, S278–S287.
- Dibble, H.L., Sandgathe, D., Goldberg, P., McPherron, S., Aldeias, V., 2018. Were western European Neandertals able to make fire? J. Paleolit. Archaeol. 1, 54–79.
- Diefendorf, A.F., Freeman, K.H., Wing, S.L., 2012. Distribution and carbon isotope patterns of diterpenoids and triterpenoids in modern temperate C3 trees and their geochemical significance. Geochim. Cosmochim. Acta 85, 342-356.
- Diefendorf, A.F., Freeman, K.H., Wing, S.L., Graham, H.V., 2011. Production of n-alkyl lipids in living plants and implications for the geologic past. Geochim. Cosmochim. Acta 75, 7472–7485.
- Diefendorf, A.F., Leslie, A.B., Wing, S.L., 2015a. Leaf wax composition and carbon isotopes vary among major conifer groups. Geochim. Cosmochim. Acta 170, 145–156.
- Diefendorf, A.F., Sberna, D.T., Taylor, D.W., 2015b. Effect of thermal maturation on plant-derived 1095 1096 terpenoids and leaf wax *n*-alkyl components. Org. Geochem. 89–90, 61–70.
 - Doerr, S.H., Santín, C., Merino, A., Belcher, C.M., Baxter, G., 2018. Fire as a removal mechanism of pyrogenic carbon from the environment: Effects of fire and pyrogenic carbon characteristics. Front. Earth Sci. 6, 127.
- 1100 Dudd, S.N., Regert, M., Evershed, R.P., 1998. Assessing microbial lipid contributions during laboratory 1101 degradations of fats and oils and pure triacylglycerols absorbed in ceramic potsherds. Org. Geochem. 29, 1345-1354. 1102
 - Eckmeier, E., Wiesenberg, G.L., 2009. Short-chain n-alkanes (C16-20) in ancient soil are useful molecular markers for prehistoric biomass burning. J. Archaeol. Sci. 36, 1590–1596.
- 1105 Eerkens, J.W., 2005. GC-MS analysis and fatty acid ratios of archaeological potsherds from the western 1106 Great Basin of north America. Archaeometry 47, 83–102.
- 1107 Eglinton, G., Hamilton, R.J., 1967. Leaf epicuticular waxes: The waxy outer surfaces of most plants 1108 display a wide diversity of fine structure and chemical constituents. Science 156, 1322–1335.

- Evershed, R.P., 2008. Organic residue analysis in archaeology: The archaeological biomarker revolution. Archaeometry 50, 895–924.
- Evershed, R.P., Copley, M.S., Dickson, L., Hansel, F.A., 2008. Experimental evidence for the processing of marine animal products and other commodities containing polyunsaturated fatty acids in pottery vessels. Archaeometry 50, 101–113.
- Fabre, L., 1996. Le charbonnage historique de la chênaie à "Quercus ilex L." (Languedoc, France) : conséquences écologiques (PhD). Université des sciences et techniques de Montpellier 2, Montpellier.
- Fernández Peris, J., González, V.B., Blasco, R., Cuartero, F., Fluck, H., Sañudo, P., Verdasco, C., 2012.
 The earliest evidence of hearths in Southern Europe: The case of Bolomor Cave (Valencia, Spain). Quat. Int. 247, 267–277.
- Fernandez-Jalvo, Y., Avery, D.M., 2015. Pleistocene Micromammals and Their Predators at Wonderwerk Cave, South Africa. Afr. Archaeol. Rev. 32, 751–791.
- Ferrio, J.P., Alonso, N., López, J.B., Araus, J.L., Voltas, J., 2006. Carbon isotope composition of fossil charcoal reveals aridity changes in the NW Mediterranean Basin. Glob. Chang. Biol. 12, 1253–124 1266.
- French, M.W., Worden, R.H., 2013. Orientation of microcrystalline quartz in the Fontainebleau Formation, Paris Basin and why it preserves porosity. Sediment. Geol. 284–285, 149–158.

1130

1153

- Glaser, B., Balashov, E., Haumaier, L., Guggenberger, G., Zech, W., 2000. Black carbon in density fractions of anthropogenic soils of the Brazilian Amazon region. Org. Geochem. 31, 669–678.
 - Glaser, B., Haumaier, L., Guggenberger, G., Zech, W., 1998. Black carbon in soils: the use of benzenecarboxylic acids as specific markers. Org. Geochem. 29, 811–819.
- González-Pérez, J.A., González-Vila, F.J., González-Vázquez, R., Arias, M.E., Rodríguez, J., Knicker, H., 2008. Use of multiple biogeochemical parameters to monitor the recovery of soils after forest fires. Org. Geochem. 39, 940–944.
- Goren-Inbar, N., Alperson, N., Kislev, M.E., Simchoni, O., Melamed, Y., Ben-Nun, A., Werker, E., 2004. Evidence of hominin control of fire at Gesher Benot Ya'aqov, Israel. Science 304, 725–727.
- Gowlett, J.A.J., 2016. The discovery of fire by humans: a long and convoluted process. Philos. Trans. R. Soc. Lond. B Biol. Sci. 371, 20150164.
- Hamer, U., Marschner, B., Brodowski, S., Amelung, W., 2004. Interactive priming of black carbon and glucose mineralisation. Org. Geochem. 35, 823–830.
- 1140 Hammes, K., Schmidt, M.W.I., Smernik, R.J., Currie, L.A., Ball, W.P., Nguyen, T.H., Louchouarn, P., Houel, S., Gustafsson, Ö., Elmquist, M., Cornelissen, G., Skjemstad, J.O., Masiello, C.A., Song, 1141 1142 J., Peng, P., Mitra, S., Dunn, J.C., Hatcher, P.G., Hockaday, W.C., Smith, D.M., Hartkopf-Fröder, 1143 C., Böhmer, A., Lüer, B., Huebert, B.J., Amelung, W., Brodowski, S., Huang, L., Zhang, W., 1144 Gschwend, P.M., Flores-Cervantes, D.X., Largeau, C., Rouzaud, J.-N., Rumpel, C., 1145 Guggenberger, G., Kaiser, K., Rodionov, A., Gonzalez-Vila, F.J., Gonzalez-Perez, J.A., de la Rosa, 1146 J.M., Manning, D.A.C., López-Capél, E., Ding, L., 2007. Comparison of quantification methods 1147 to measure fire-derived (black/elemental) carbon in soils and sediments using reference 1148 materials from soil, water, sediment and the atmosphere. Global Biogeochem. Cycles 21, 1149 GB3016.
- 1150 Hansel, F.A., Copley, M.S., Madureira, L.A.S., Evershed, R.P., 2004. Thermally produced ω -(o1151 alkylphenyl)alkanoic acids provide evidence for the processing of marine products in
 1152 archaeological pottery vessels. Tetrahedron Lett. 45, 2999–3002.
 - Helmens, K.F., 2014. The Last Interglacial–Glacial cycle (MIS 5–2) re-examined based on long proxy records from central and northern Europe. Quat. Sci. Rev. 86, 115–143.
- Henry, A., 2011. Paléoenvironnements et gestion des combustibles au Mésolithique dans le sud de la France: anthracologie, ethnoarchéologie et expérimentation (PhD). Université Nice Sophia Antipolis, Nice, France.
- Henry, A., Théry-Parisot, I., 2014. From Evenk campfires to prehistoric hearths: charcoal analysis as a tool for identifying the use of rotten wood as fuel. J. Archaeol. Sci. 52, 321–336.

- Herries, A., 2006. Archaeomagnetic evidence for climate change at Sibudu Cave. Southern African Humanities 18, 131–147.
- Hilscher, A., Heister, K., Siewert, C., Knicker, H., 2009. Mineralisation and structural changes during the initial phase of microbial degradation of pyrogenic plant residues in soil. Org. Geochem. 40, 332–342.
- Hjulström, B., Isaksson, S., Hennius, A., 2006. Organic geochemical evidence for pine tar production in middle eastern Sweden during the Roman iron age. J. Archaeol. Sci. 33, 283–294.
- 1167 Hobley, E., 2019. Vertical distribution of soil pyrogenic matter: A review. Pedosphere 29, 137–149.
- Hoefs, M.J.L., Rijpstra, W.I.C., Sinninghe Damsté, J.S., 2002. The influence of oxic degradation on the sedimentary biomarker record I: evidence from Madeira Abyssal Plain turbidites. Geochim. Cosmochim. Acta 66, 2719–2735.
- Jambrina-Enríquez, M., Herrera-Herrera, A.V., Mallol, C., 2018. Wax lipids in fresh and charred anatomical parts of the *Celtis australis* tree: Insights on paleofire interpretation. Org. Geochem. 122, 147–160.
- Jambrina-Enríquez, M., Herrera-Herrera, A.V., Rodríguez de Vera, C., Leierer, L., Connolly, R., Mallol, C., 2019. *n*-Alkyl nitriles and compound-specific carbon isotope analysis of lipid combustion residues from Neanderthal and experimental hearths: Identifying sources of organic compounds and combustion temperatures. Quat. Sci. Rev. 222, 105899.
 - Jian, M., Berhe, A.A., Berli, M., Ghezzehei, T.A., 2018. Vulnerability of physically protected soil organic carbon to loss under low severity fires. Front. Environ. Sci. 6, 368737.
- 1180 Kappenberg, A., Bläsing, M., Lehndorff, E., Amelung, W., 2016. Black carbon assessment using benzene 1181 polycarboxylic acids: Limitations for organic-rich matrices. Org. Geochem. 94, 47–51.

1179

11841185

1186

1187

1188

1189

1190

- 1182 Kappenberg, A., Lehndorff, E., Pickarski, N., Litt, T., Amelung, W., 2019. Solar controls of fire events 1183 during the past 600,000 years. Quat. Sci. Rev. 208, 97–104.
 - Knicker, H., 2011. Pyrogenic organic matter in soil: Its origin and occurrence, its chemistry and survival in soil environments. Quat. Int. 243, 251–263.
 - Knicker, H., Hilscher, A., de la Rosa, J.M., González-Pérez, J.A., González-Vila, F.J., 2013. Modification of biomarkers in pyrogenic organic matter during the initial phase of charcoal biodegradation in soils. Geoderma 197–198, 43–50.
 - Koch, T.J., Saurel, M., Bocquillon, H., Pisani, D.F., Bonnabel, L., Little, A., Stacey, R., Rageot, M., Regert, M., 2024. Differences in birch tar composition are explained by adhesive function in the central European Iron Age. PLoS One 19, e0301103.
- Kolattukudy, P.E., 1980. Biopolyester membranes of plants: cutin and suberin. Science 208, 990–1000. Kolattukudy, P.E., 2001. Polyesters in higher plants. Adv. Biochem. Eng. Biotechnol. 71, 1–49.
 - Kolattukudy, P.E., 2001. Polyesters in higher plants. Adv. Biochem. Eng. Biotechnol. 71, 1–49.
 Komarek, E.V., Komarek, B.B., Carlysle, T.C., 1973. The ecology of smoke particulates and charcoal
- Komarek, E.V., Komarek, B.B., Carlysle, T.C., 1973. The ecology of smoke particulates and charcoal residues from forest and grassland fires: a preliminary atlas. Tall Timbers Research Station, Tallahassee, FL.
- Lacarrière, J., Bodu, P., Julien, M.-A., Dumarçay, G., Goutas, N., Lejay, M., Peschaux, C., Naton, H.-G.,
 Théry-Parisot, I., Vasiliu, L., 2015. Les Bossats (Ormesson, Paris basin, France): A new early
 Gravettian bison processing camp. Quat. Int. 359–360, 520–534.
- Lejay, M., Alexis, M.A., Quénéa, K., Anquetil, C., Bon, F., 2019. The organic signature of an experimental meat-cooking fireplace: The identification of nitrogen compounds and their archaeological potential. Org. Geochem. 138, 103923.
- Lin, L.H., Simpson, M.J., 2016. Enhanced extractability of cutin- and suberin-derived organic matter with demineralization implies physical protection over chemical recalcitrance in soil. Org. Geochem. 97, 111–121.
- Lucquin, A., March, R.J., Cassen, S., 2007. Analysis of adhering organic residues of two "coupes-à-socles" from the Neolithic funerary site "La Hougue Bie" in Jersey: evidences of birch bark tar utilisation. J. Archaeol. Sci. 34, 704–710.
- Maher, B.A., 1998. Magnetic properties of modern soils and Quaternary loessic paleosols: paleoclimatic implications. Palaeogeogr. Palaeoclimatol. Palaeoecol. 137, 25–54.

- March, R.J., Lucquin, A., Joly, D., Ferreri, J.C., Muhieddine, M., 2014. Processes of formation and 1211 1212 alteration of archaeological fire structures: Complexity viewed in the light of experimental 1213 approaches. J. Archaeol. Method Theory 21, 1-45.
- 1214 Marguerie, D., Hunot, J.-Y., 2007. Charcoal analysis and dendrology: data from archaeological sites in 1215 north-western France. J. Archaeol. Sci. 34, 1417–1433.
- Marynowski, L., Scott, A.C., Zatoń, M., Parent, H., Garrido, A.C., 2011. First multi-proxy record of 1216 Jurassic wildfires from Gondwana: Evidence from the Middle Jurassic of the Neuquén Basin, 1217 1218 Argentina. Palaeogeogr. Palaeoclimatol. Palaeoecol. 299, 129–136.
- 1219 Marzi, R., Torkelson, B.E., Olson, R.K., 1993. A revised carbon preference index. Org. Geochem. 20, 1220
- 1221 McParland, L.C., Collinson, M.E., Scott, A.C., Campbell, G., 2009. The use of reflectance values for the 1222 interpretation of natural and anthropogenic charcoal assemblages. Archaeol. Anthropol. Sci. 1223
- McParland, L.C., Collinson, M.E., Scott, A.C., Campbell, G., Veal, R., 2010. Is vitrification in charcoal a 1224 1225 result of high temperature burning of wood? J. Archaeol. Sci. 37, 2679–2687.
- 1226 Moody, J.A., Shakesby, R.A., Robichaud, P.R., Cannon, S.H., Martin, D.A., 2013. Current research issues 1227 related to post-wildfire runoff and erosion processes. Earth Sci. Rev. 122, 10–37.

1229

1230

1236

1237

1238

1241

1243

1244

- Mouraux, C., Delarue, F., Bardin, J., Nguyen Tu, T.T., Bellot-Gurlet, L., Paris, C., Coubray, S., Dufraisse, A., 2022. Assessing the carbonisation temperatures recorded by ancient charcoals for δ^{13} Cbased palaeoclimate reconstruction. Sci. Rep. 12, 14662.
- 1231 Müller, U.C., Pross, J., Bibus, E., 2003. Vegetation response to rapid climate change in Central Europe during the past 140,000 yr based on evidence from the Füramoos pollen record. Quat. Res. 59, 1232 1233
- 1234 Naafs, D.F.W., van Bergen, P.F., Boogert, S.J., de Leeuw, J.W., 2004. Solvent-extractable lipids in an acid andic forest soil; variations with depth and season. Soil Biol. Biochem. 36, 297-308. 1235
 - Nezhad, M.T.K., Šamonil, P., Daněk, P., Jaroš, J., Hájek, M., Hájková, P., Jabinski, S., Meador, T.B., Roleček, J., 2024. Lipid biomarkers and stable isotopes uncover paleovegetation changes in extremely species-rich forest-steppe ecosystems, Central Europe. Environ. Res. 259, 119564.
- 1239 Nierop, K.G.J., Jansen, B., Hageman, J.A., Verstraten, J.M., 2006. The complementarity of extractable 1240 and ester-bound lipids in a soil profile under pine. Plant Soil 286, 269–285.
- Notterpek, I., Craig, O.E., Garberi, P., Lucquin, A., Théry-Parisot, I., Abiven, S., 2025. BPChAr-a Benzene 1242 Polycarboxylic Acid database to describe the molecular characteristics of laboratory-produced charcoal: Implications for soil science and archaeology. PLoS One 20, e0321584.
 - Onda, Y., Dietrich, W.E., Booker, F., 2008. Evolution of overland flow after a severe forest fire, Point Reyes, California. Catena 72, 13-20.
- 1246 Otto, A., Simoneit, B.R.T., 2001. Chemosystematics and diagenesis of terpenoids in fossil conifer 1247 species and sediment from the Eocene Zeitz formation, Saxony, Germany. Geochim. 1248 Cosmochim. Acta 65, 3505–3527.
- 1249 Otto, A., Simpson, M.J., 2006. Sources and composition of hydrolysable aliphatic lipids and phenols in 1250 soils from western Canada. Org. Geochem. 37, 385-407.
- 1251 Pignatello, J.J., Uchimiya, M., Abiven, S., 2024. Aging of biochar in soils and its implications, in: 1252 Lehmann, J., Jospeh, S. (Eds.), Biochar for Environmental Management. Routledge, London, 1253 pp. 249-276.
- 1254 Pignatello, J.J., Uchimiya, M., Abiven, S., Schmidt, M.W.I., 2015. Evolution of biochar properties in soil, 1255 in: Lehmann, J., Jospeh, S. (Eds.), Biochar for Environmental Management. Routledge, London, 1256 pp. 47-70.
- 1257 Poynter, J.G., Farrimond, P., Robinson, N., Eglinton, G., 1989. Aeolian-derived higher plant lipids in the 1258 marine sedimentary record: Links with palaeoclimate, in: Leinen, M., Sarnthein, M. (Eds.), 1259 Paleoclimatology and Paleometeorology: Modern and Past Patterns of Global Atmospheric 1260 Transport. Springer Netherlands, Dordrecht, pp. 435–462.
- 1261 Prior, J., Alvin, K.L., 1986. Structural changes on charring woods of Dichrostachys and Salix from 1262 southern Africa: The effect of moisture content. IAWA J. 7, 243–250.

- 1263 Pyne, S.J., Andrews, P.L., Laven, R.D., 1996. Introduction to Wildland Fire. J. Wiley and Sons, New York.
- Quénéa, K., Largeau, C., Derenne, S., Spaccini, R., Bardoux, G., Mariotti, A., 2006. Molecular and isotopic study of lipids in particle size fractions of a sandy cultivated soil (Cestas cultivation sequence, southwest France): Sources, degradation, and comparison with Cestas forest soil.

 Org. Geochem. 37, 20–44.
- Rageot, M., Théry-Parisot, I., Beyries, S., Lepère, C., Carré, A., Mazuy, A., Filippi, J.-J., Fernandez, X., Binder, D., Regert, M., 2019. Birch bark tar production: Experimental and biomolecular approaches to the study of a common and widely used prehistoric adhesive. J. Archaeol. Method Theory 26, 276–312.
- Rasmussen, S.O., Bigler, M., Blockley, S.P., Blunier, T., Buchardt, S.L., Clausen, H.B., Cvijanovic, I., Dahl-Jensen, D., Johnsen, S.J., Fischer, H., Gkinis, V., Guillevic, M., Hoek, W.Z., Lowe, J.J., Pedro, J.B., Popp, T., Seierstad, I.K., Steffensen, J.P., Svensson, A.M., Vallelonga, P., Vinther, B.M., Walker, M.J.C., Wheatley, J.J., Winstrup, M., 2014. A stratigraphic framework for abrupt climatic changes during the Last Glacial period based on three synchronized Greenland ice-core records: refining and extending the INTIMATE event stratigraphy. Quat. Sci. Rev. 106, 14–28.
- Rein, G., Cleaver, N., Ashton, C., Pironi, P., Torero, J.L., 2008. The severity of smouldering peat fires and damage to the forest soil. Catena 74, 304–309.

1281

1282

1283

1284

1285

1286

12871288

1297

1298

- Rhodes, S.E., Walker, M.J., López-Jiménez, A., López-Martínez, M., Haber-Uriarte, M., Fernández-Jalvo, Y., Chazan, M., 2016. Fire in the Early Palaeolithic: Evidence from burnt small mammal bones at Cueva Negra del Estrecho del Río Quípar, Murcia, Spain. J. Archaeol. Sci. Rep. 9, 427–436.
- Roebroeks, W., Villa, P., 2011. On the earliest evidence for habitual use of fire in Europe. Proc. Natl. Acad. Sci. U. S. A. 108, 5209–5214.
- Rommerskirchen, F., Eglinton, G., Dupont, L., Güntner, U., Wenzel, C., Rullkötter, J., 2003. A north to south transect of Holocene southeast Atlantic continental margin sediments: Relationship between aerosol transport and compound-specific δ^{13} C land plant biomarker and pollen records. Geochem. Geophys. Geosyst. 4, 1101.
- Rosell, J., Blasco, R., 2019. The early use of fire among Neanderthals from a zooarchaeological perspective. Quat. Sci. Rev. 217, 268–283.
- Rumpel, C., Leifeld, J., Santin, C., Doerr, S., 2015. Movement of biochar in the environment, in: Lehmann, J., Joseph, S. (Eds.), Biochar for Environmental Management. Routledge, London, pp. 95–120.
- Rundel, P.W., 1981. Fire as an Ecological Factor, in: Lange, O.L., Nobel, P.S., Osmond, C.B., Ziegler, H. (Eds.), Physiological Plant Ecology I: Responses to the Physical Environment, Encyclopedia of Plant Physiology. Springer-Verlag, Berlin, pp. 501–538.
 - Rundel, P.W., 1983. Impact of fire on nutrient cycles in Mediterranean-type ecosystems with reference to chaparral, in: Kruger, F.J., Mitchell, D.T., Jarvis, J.U.M. (Eds.), Mediterranean-Type Ecosystems: The Role of Nutrients, Ecological Studies. Springer-Verlag, Berlin, pp. 192–207.
- Saiz, G., Goodrick, I., Wurster, C., Nelson, P.N., Wynn, J., Bird, M., 2018. Preferential production and transport of grass-derived pyrogenic carbon in NE-Australian Savanna ecosystems. Front. Earth Sci. 5, 115.
- Sandgathe, D.M., 2017. Identifying and describing pattern and process in the evolution of hominin use of fire. Curr. Anthropol. 58, S360–S370.
- Sandgathe, D.M., Dibble, H.L., Goldberg, P., McPherron, S.P., Turq, A., Niven, L., Hodgkins, A.J., 2011.
 On the role of fire in Neandertal adaptations in western Europe: Evidence from Pech de l'Azé
 and Roc de Marsal, France. PaleoAnthropology 2011, 216–242.
- Santos, F., Bird, J.A., Asefaw Berhe, A., 2022. Dissolved pyrogenic carbon leaching in soil: Effects of soil depth and pyrolysis temperature. Geoderma 424, 116011.
- Sanz, M., Daura, J., Cabanes, D., Égüez, N., Carrancho, Á., Badal, E., Souto, P., Rodrigues, F., Zilhão, J., 2020. Early evidence of fire in south-western Europe: the Acheulean site of Gruta da Aroeira (Torres Novas, Portugal). Sci. Rep. 10, 12053.

- Sarangi, V., Roy, S., Sanyal, P., 2022. Effect of burning on the distribution pattern and isotopic composition of plant biomolecules: Implications for paleoecological studies. Geochim. Cosmochim. Acta 318, 305–327.
- Schäfer, I.K., Lanny, V., Franke, J., Eglinton, T.I., Zech, M., Vysloužilová, B., Zech, R., 2016. Leaf waxes in litter and topsoils along a European transect. SOIL 2, 551–564.
- Schiedung, M., Bellè, S.-L., Sigmund, G., Kalbitz, K., Abiven, S., 2020. Vertical mobility of pyrogenic organic matter in soils: a column experiment. Biogeosciences 17, 6457–6474.
- Scott, A.C., 2010. Charcoal recognition, taphonomy and uses in palaeoenvironmental analysis.
 Palaeogeogr. Palaeoclimatol. Palaeoecol. 291, 11–39.
- Shakesby, R.A., 2011. Post-wildfire soil erosion in the Mediterranean: Review and future research directions. Earth Sci. Rev. 105, 71–100.
- Shimelmitz, R., Kuhn, S.L., Jelinek, A.J., Ronen, A., Clark, A.E., Weinstein-Evron, M., 2014. "Fire at will": the emergence of habitual fire use 350,000 years ago. J. Hum. Evol. 77, 196–203.
- Sievers, C., Wadley, L., 2008. Going underground: experimental carbonization of fruiting structures under hearths. J. Archaeol. Sci. 35, 2909–2917.
- 1328 Simoneit, B., 1986. Cyclic terpenoids of the geosphere. Meth. Geochem. Geophys. 24, 43–99.

1334

1335

1339

1340

1341

1347

1348

1349

13501351

1359

- Singh, N., Abiven, S., Torn, M.S., Schmidt, M.W.I., 2012. Fire-derived organic carbon in soil turns over on a centennial scale. Biogeosciences 9, 2847–2857.
- Spielvogel, S., Prietzel, J., Leide, J., Riedel, M., Zemke, J., Kögel-Knabner, I., 2014. Distribution of cutin and suberin biomarkers under forest trees with different root systems. Plant Soil 381, 95–110.
 - Spokas, K.A., Novak, J.M., Masiello, C.A., Johnson, M.G., Colosky, E.C., Ippolito, J.A., Trigo, C., 2014. Physical disintegration of biochar: An overlooked process. Environ. Sci. Technol. Lett. 1, 326–332.
- Stahlschmidt, M.C., Miller, C.E., Ligouis, B., Hambach, U., Goldberg, P., Berna, F., Richter, D., Urban, B.,
 Serangeli, J., Conard, N.J., 2015. On the evidence for human use and control of fire at
 Schöningen. J. Hum. Evol. 89, 181–201.
 - Stancampiano, L.M., Rubio-Jara, S., Panera, J., Uribelarrea, D., Pérez-González, A., Magill, C.R., 2023.

 Organic geochemical evidence of human-controlled fires at Acheulean site of Valdocarros II (Spain, 245 kya). Sci. Rep. 13, 7119.
- Stocks, B.J., Kauffman, J.B., 1997. Biomass Consumption and Behavior of Wildland Fires in Boreal, Temperate, and Tropical Ecosystems: Parameters Necessary to Interpret Historic Fire Regimes and Future Fire Scenarios, in: Clark, J.S., Cachier, H., Goldammer, J.G., Stocks, B. (Eds.), Sediment Records of Biomass Burning and Global Change. Springer-Verlag, Berlin, pp. 169– 188.
 - Stoof, C.R., Gevaert, A.I., Baver, C., Hassanpour, B., Morales, V.L., Zhang, W., Martin, D., Giri, S.K., Steenhuis, T.S., 2016. Can pore-clogging by ash explain post-fire runoff? Int. J. Wildland Fire 25, 294.
 - Théry-Parisot, I., 2001. Economie des combustibles au paléolithique: expérimentation, taphonomie, anthracologie. Dossiers de documentation archéologique n° 20. CNRS Editions.
- Théry-Parisot, I., Audiard, B., Carre, A., Coli, V.-L., Garberi, P., Lavalette, A., 2025. Fire and heat, from hearth to charcoal: An experimental approach to temperature in the context of Palaeolithic hearths. J. Archaeol. Sci. Rep. 61, 104977.
- Théry-Parisot, I., Henry, A., 2012. Seasoned or green? Radial cracks analysis as a method for identifying the use of green wood as fuel in archaeological charcoal. J. Archaeol. Sci. 39, 381–388.
- Thomas, C.L., Jansen, B., van Loon, E.E., Wiesenberg, G.L.B., 2021. Transformation of *n*-alkanes from plant to soil: a review. SOIL 7, 785–809.
 - Usup, A., Hashimoto, Y., Takahashi, H., Hayasaka, H., 2004. Combustion and thermal characteristics of peat fire in tropical peatland in Central Kalimantan, Indonesia. Tropics 14, 1–19.
- Vaezzadeh, V., Zhong, G., Zhang, G., 2023. Benzene polycarboxylic acids as molecular markers of black carbon: Progresses and challenges. Chemosphere 341, 140112.

- van Bergen, P.F., Bull, I.D., Poulton, P.R., Evershed, R.P., 1997. Organic geochemical studies of soils from the Rothamsted Classical Experiments—I. Total lipid extracts, solvent insoluble residues and humic acids from Broadbalk Wilderness. Org. Geochem. 26, 117–135.
- 1366 Van Wagner, C.E., 1977. Conditions for the start and spread of crown fire. Can. J. For. Res. 7, 23–34.
- Vidal-Matutano, P., Alberto-Barroso, V., Marrero, E., García, J.C., Pou, S., de la Rosa, M.A., 2019.
 Vitrified wood charcoal and burnt bones from the pre-Hispanic site of Chasogo (Tenerife, Canary Islands, Spain). J. Archaeol. Sci. Rep. 28, 102005.
- 1370 Vidal-Matutano, P., Henry, A., Carrión-Marco, Y., Allué, E., 2020. Disentangling human from natural 1371 factors: Taphonomical value of microanatomical features on archaeological wood and charcoal 1372 assemblages. J. Archaeol. Sci. Rep. 31, 102328.
- 1373 Vidal-Matutano, P., Henry, A., Théry-Parisot, I., 2017. Dead wood gathering among Neanderthal 1374 groups: Charcoal evidence from Abric del Pastor and El Salt (Eastern Iberia). J. Archaeol. Sci. 1375 80, 109–121.
- Volkman, J.K., 2005. Sterols and other triterpenoids: source specificity and evolution of biosynthetic pathways. Org. Geochem. 36, 139–159.
- Walker, M.J., Anesin, D., Angelucci, D.E., Avilés-Fernández, A., Berna, F., Buitrago-López, A.T.,
 Fernández-Jalvo, Y., Haber-Uriarte, M., López-Jiménez, A., López-Martínez, M., Martín-Lerma,
 I., Ortega-Rodrigáñez, J., Polo-Camacho, J.-L., Rhodes, S.E., Richter, D., Rodríguez-Estrella, T.,
 Schwenninger, J.-L., Skinner, A.R., 2016. Combustion at the late Early Pleistocene site of Cueva
 Negra del Estrecho del Río Quípar (Murcia, Spain). Antiquity 90, 571–589.
 - Watts, A.C., Kobziar, L.N., 2013. Smoldering combustion and ground fires: Ecological effects and multiscale significance. Fire Ecol. 9, 124–132.
- Wiesenberg, G.L., Gocke, M., Kuzyakov, Y., 2010. Fast incorporation of root-derived lipids and fatty
 acids into soil Evidence from a short term multiple pulse labelling experiment. Org. Geochem.
 41, 1049–1055.

1384

1390

1391

1392

- Wiesenberg, G.L., Lehndorff, E., Schwark, L., 2009. Thermal degradation of rye and maize straw: Lipid pattern changes as a function of temperature. Org. Geochem. 40, 167–174.
 - Wiesenberg, G.L., Schneckenberger, K., Schwark, L., Kuzyakov, Y., 2012. Use of molecular ratios to identify changes in fatty acid composition of Miscanthus×giganteus (Greef et Deu.) plant tissue, rhizosphere and root-free soil during a laboratory experiment. Org. Geochem. 46, 1–11.
- Wohlfarth, B., 2013. A review of Early Weichselian climate (MIS 5d-a) in Europe. Department of Geological Sciences, Stockholm University.
- Woillard, G.M., 1978. Grande Pile peat bog: A continuous pollen record for the last 140,000 years.

 Quat. Res. 9, 1–21.
- Wolf, M., Lehndorff, E., Wiesenberg, G.L.B., Stockhausen, M., Schwark, L., Amelung, W., 2013. Towards reconstruction of past fire regimes from geochemical analysis of charcoal. Org. Geochem. 55, 1400 11–21.
- Wöstehoff, L., Kappenberg, A., Lehndorff, E., Wagner, B., Panagiotopoulos, K., Amelung, W., 2023. An
 upper Pleistocene and Holocene black carbon-related fire record from the SW Balkans.
 Paleoceanogr. Paleoclimatology 38, e2022PA004579.
- Wöstehoff, L., Kindermann, K., Amelung, W., Kappenberg, A., Henselowsky, F., Lehndorff, E., 2022.
 Anthropogenic fire fingerprints in Late Pleistocene and Holocene sediments of Sodmein Cave,
 Egypt. J. Archaeol. Sci. Rep. 42, 103411.
- Zech, R., Zech, M., Marković, S., Hambach, U., Huang, Y., 2013. Humid glacials, arid interglacials?
 Critical thoughts on pedogenesis and paleoclimate based on multi-proxy analyses of the loess–
 paleosol sequence Crvenka, Northern Serbia. Palaeogeogr. Palaeoclimatol. Palaeoecol. 387,
 165–175.
- Zhang, Y., Peng, T., Yu, J., Su, Y., Liu, Z., 2021. Natural and anthropogenically driven changes in the *n*-alkanols of lake sediments and implications for their use in paleoenvironmental studies of lakes. Catena 207, 105591.

Zhang, Z., Zhao, M., Eglinton, G., Lu, H., Huang, C., 2006. Leaf wax lipids as paleovegetational and 1414 1415 paleoenvironmental proxies for the Chinese Loess Plateau over the last 170kyr. Quat. Sci. Rev. 1416 25, 575-594. 1417 Zheng, Y., Xie, S., Liu, X., Zhou, W., Meyers, P.A., 2009. n-alkanol ratios as proxies of paleovegetation and paleoclimate in a peat-lacustrine core in southern China since the last deglaciation. Front. 1418 1419 Earth Sci. China 3, 445–451. 1420 Zheng, Y., Zhou, W., Meyers, P.A., Xie, S., 2007. Lipid biomarkers in the Zoigê-Hongyuan peat deposit: 1421 Indicators of Holocene climate changes in West China. Org. Geochem. 38, 1927–1940. 1422 Zhou, W., Zheng, Y., Meyers, P.A., Jull, A.J.T., Xie, S., 2010. Postglacial climate-change record in 1423 biomarker lipid compositions of the Hani peat sequence, Northeastern China. Earth Planet. Sci. 1424 Lett. 294, 37-46. 1425 **Acknowledgements** 1426 1427 This project has received funding from the European Union's Horizon 2020 research and innovation 1428 programme under the Marie Skłodowska-Curie grant agreement No 956351. **Data availability** 1429 1430 All data is contained within the submission. Table S1 and raw chromatograms are also available for

download from the Zenodo repository (doi: 10.5281/zenodo.15113743).